

Selective Ni-Catalyzed Hydroboration of CO₂ to the Formaldehyde Level Enabled by New PSiP Ligation

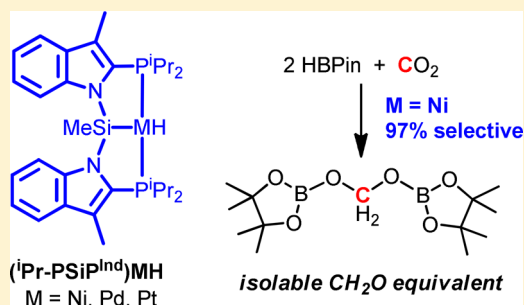
Luke J. Murphy,[†] Helia Hollenhorst,[†] Robert McDonald,^{‡,§} Michael Ferguson,^{‡,§} Michael D. Lumsden,[†] and Laura Turculet^{*,†,§}

[†]Department of Chemistry, Dalhousie University, 6274 Coburg Road, P.O. Box 15000, Halifax, Nova Scotia, Canada B3H 4R2

[‡]X-Ray Crystallography Laboratory, Department of Chemistry, University of Alberta, Edmonton, Alberta, Canada T6G 2G2

Supporting Information

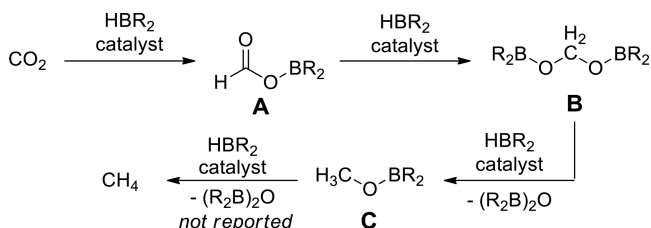
ABSTRACT: The synthesis and characterization of group 10 metal pincer complexes supported by a new bis(indolylphosphino)silyl ligand are described, including the synthesis of Ni, Pd, and Pt hydride species. Solution NMR and single-crystal X-ray data revealed that a significant amount of structural variability is possible for such hydride complexes, particularly in the case of Ni, where terminal Ni-H as well as complexes involving η^2 -SiH coordination are both accessible and may even coexist, in ratios dependent on factors such as the nature of additional coligands, including N₂ from the reaction atmosphere, as well as solvent and temperature. Nickel and palladium hydride complexes of this new ligand were found to exhibit divergent selectivity in the catalytic hydroboration of CO₂ with pinacolborane (HBPin). While the Pd catalyst exhibited moderate activity for CO₂ hydroboration to the formate level, the analogous Ni species exhibited unprecedented selectivity (97%) for hydroboration of CO₂ to the formaldehyde level to provide the bis(boryl)acetal PinBOCH₂OBPIn in high yield, under mild conditions. The HBPin-derived bis(boryl)acetal can be successfully isolated and utilized as a source of methylene for the formation of C–N and C–P bonds.



INTRODUCTION

Significant effort has been made in recent years to develop efficient methods of utilizing CO₂ as a C1 source for chemical synthesis.¹ Both transition-metal and main-group catalysts have been applied in this regard to achieve transformations such as the reduction of CO₂ to formic acid, methanol, or methane, as well as coupling reactions involving alkenes and alkynes.² While H₂ represents the most attractive reductant from an atom economy point of view, the hydroboration of CO₂ has received considerable attention and has been shown to be a versatile reaction that can yield a variety of products along the reduction pathway from CO₂ to methane (Scheme 1).³ From a practical perspective, it must be noted that this reaction makes use of a stoichiometric borane reductant that cannot be efficiently regenerated. However, the hydroboration of CO₂ is of interest

Scheme 1. Stepwise Hydroboration of CO₂ to Boryl Formate (A), Bis(boryl)acetal (B), and Methoxyborane (C) Species and Finally to Methane (Not Yet Reported)



from a fundamental reactivity perspective. In the majority of cases, the products of CO₂ hydroboration are boryl formate species (A, resulting from single reduction)⁴ or methoxyborane species (C, resulting from triple reduction)⁵ that can be hydrolyzed to yield formic acid or methanol, respectively. By comparison, *double* reduction to the corresponding bis(boryl)acetal (B) is relatively rare, and full reduction to methane using hydroboranes has remained elusive.⁷

The selective formation of a bis(boryl)acetal product (B) by a *double* CO₂ reduction process is particularly intriguing, as it represents a reduction of CO₂ to the formaldehyde level. Formaldehyde has been identified as a “missing link” in homogeneous CO₂ reduction catalysis that may serve as a useful C1 synthon for the formation of various E–C bonds (E = main-group element).^{6b,8} The first report of double hydroboration of CO₂ was disclosed by Bontemps, Sabo-Etienne, and co-workers^{6a} in the course of investigations involving Ru-catalyzed CO₂ reduction with pinacolborane (HBPin). A number of reduction products were identified in various proportions, including A–C and PinBOCH₂(OCOH), where the last species results from a rare coupling of two molecules of CO₂. When Fe(H)₂(dmpe)₂ (dmpe = 1,2-bis(dimethylphosphino)ethane) was used as a catalyst, it was observed that, while the use of catecholborane (HBCat) as reductant led to selective formation of the corresponding

Received: June 30, 2017

methoxyborane (C) in moderate yield, the use of HBPIn and 9-BBN (9-borabicyclo[3.3.1]nonane) as reductants favored the formation of the corresponding bis(boryl)acetals (B).^{6c} The in situ generated bis(boryl)acetal derived from 9-BBN was shown to be an effective methylene transfer reagent that could be utilized for the formation of C–N, C–O, and C–C bonds, thereby providing new avenues for the utilization of CO₂ in synthesis.^{6e} Since these initial reports by Bontemps, Sabo-Etienne, and co-workers, a handful of other CO₂ hydroboration studies have reported the generation of product mixtures containing bis(boryl)acetals, but these studies have not focused on optimizing the formation of this double-reduction product.^{5c,e,6d}

Our group has had significant interest in the reactivity and catalytic applications of transition-metal pincer complexes, including the utility of such complexes as catalysts for CO₂ reduction processes. In this regard, we have previously reported on the catalytic hydrosilylation of CO₂ mediated by Pd and Pt silyl pincer complexes supported by κ^3 -(2-Cy₂PC₆H₄)₂SiMe (Cy-PSiP) ligation developed in our group.^{7c} Group 10 metal pincer complexes have also found application as effective catalysts for both single (formate level) and triple (methanol level) CO₂ hydroboration processes. Guan and co-workers^{5a} were the first to report CO₂ hydroboration to the methanol level catalyzed by a POCOP (POCOP = 2,6-(^tBu₂PO)₂C₆H₃) pincer complex of Ni. A subsequent computational study underlined the strong influence that both steric congestion at the Ni center and the identity of the borane reductant have on catalytic efficiency.⁹ More recently, Hazari and co-workers^{4b} reported on the hydroboration of CO₂ with HBPIn to the formate level catalyzed by (Cy-PSiP)PdH. The system operates under mild conditions and achieved the highest turnover numbers to date for hydroboration of CO₂ to the formate level. While these examples demonstrate that tuning of parameters such as catalyst structure and borane source can have a significant effect on the selectivity of the hydroboration process, no examples of related pincer species that are both productive and highly selective for the double hydroboration of CO₂ to the formaldehyde level have been reported.¹⁰

Given the relative rarity of catalyst platforms that can selectively reduce CO₂ to the formaldehyde level, the development of new catalysts for this transformation is of fundamental interest both from an organometallic reactivity perspective and in an effort to develop useful transformations of CO₂. In this context, we report herein the development of a new bis(indolylphosphino)silyl PSiP ligand (Figure 1), along

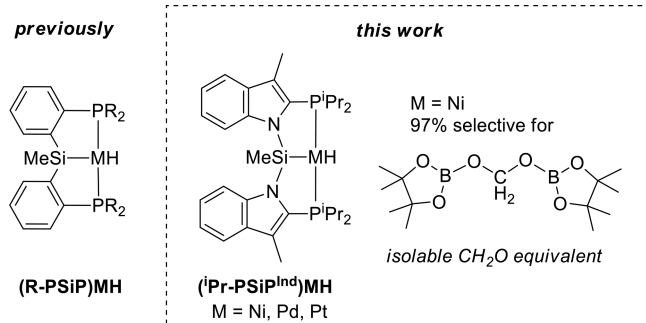


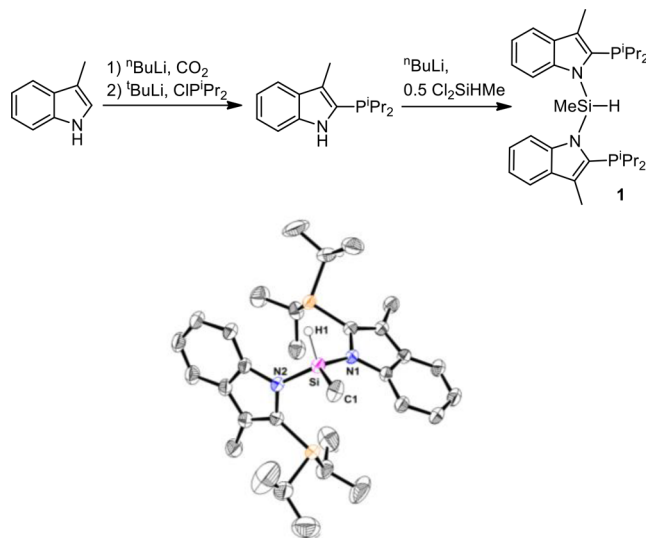
Figure 1. Previously reported bis(phosphino)silyl group 10 metal hydride complexes active in CO₂ hydroboration catalysis and new bis(indolylphosphino)silyl complexes of the type reported herein.

with the synthesis and characterization of group 10 pincer complexes of this ligand. We focused on the preparation of metal hydride derivatives, as these have been shown to be key species for CO₂ reduction catalysis. Nickel and palladium hydride complexes of this new ligand are shown to exhibit divergent selectivity in the catalytic hydroboration of CO₂ with HBPIn. Interestingly, while the Pd catalyst is selective for the formation of the corresponding boryl formate product, the analogous Ni species leads almost exclusively (97% selectivity) to the formation of the bis(boryl)acetal (B), in a manner that was not achieved by use of previously reported group 10 catalysts, including those featuring bis(phosphino)silyl pincer ligation. We further demonstrate that the HBPIn-derived bis(boryl)acetal can be successfully isolated and utilized as a source of methylene for the formation of E–C bonds.

RESULTS AND DISCUSSION

Ligand Synthesis. In previous work, our group has demonstrated that bis(phosphino)silyl PSiP pincer complexes can facilitate a variety of challenging bond activation processes, including C–H and N–H bond oxidative addition,¹¹ as well as the reduction of carbon dioxide to methane using tertiary silanes.^{7c} In an effort to understand better the effects of PSiP ancillary ligand modifications on the reactivity of the ensuing complexes, we sought to prepare a new PSiP variant featuring a bis(indolylphosphino) motif (Scheme 2). The tertiary silane

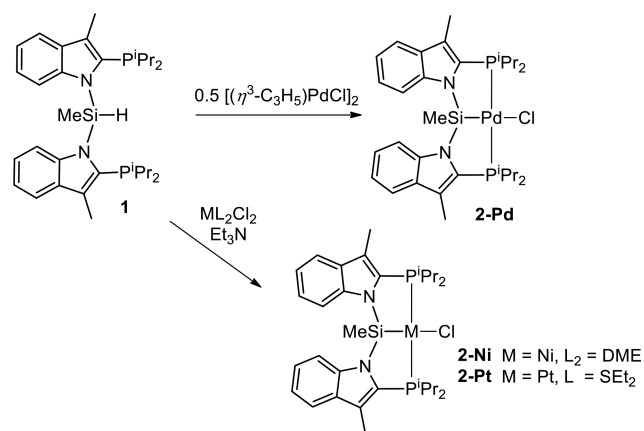
Scheme 2. Synthesis of Bis(indolylphosphino)silane Ligand Precursors and Single-Crystal X-ray Structure of 1^a



^aInset crystal structure shown with 50% thermal ellipsoids and with selected hydrogen atoms omitted for clarity.

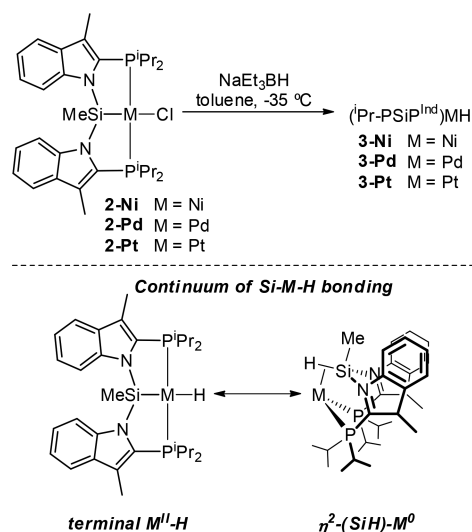
ligand precursor 1 ((ⁱPr-PSiP^{Ind})H) was readily prepared from commercially available 3-methylindole using a synthetic strategy analogous to that employed by Reek and co-workers¹² for the preparation of INDOLPhos ligands and was isolated as a white solid in 53% overall yield (over three synthetic steps). The X-ray crystal structure of 1 confirmed the connectivity in this molecule (Scheme 2).

Synthesis of Group 10 Metal Complexes. Group 10 metal chloride complexes of the type (ⁱPr-PSiP^{Ind})MCl (M = Ni (2-Ni), Pd (2-Pd), Pt (2-Pt)) were prepared in high yield (Scheme 3). Despite diligent efforts to obtain these complexes

Scheme 3. Synthesis of (*i*Pr-PSiP^{Ind})MCl (M = Ni, Pd, Pt) Complexes

and related derivatives (vide infra) solvent-free in analytically pure form, in several cases the isolated compounds were found to tenaciously retain solvent even after prolonged exposure to vacuum. Nonetheless, spectroscopic and X-ray crystallographic data (Figure 2) serve to unequivocally confirm the identity of the target compounds. All three chloride complexes exhibit distorted-square-planar coordination geometry about the metal center with spectroscopic features comparable to those of related PSiP complexes of this type.¹³ The synthesis of hydride derivatives was pursued subsequently, with the goal of accessing species capable of CO₂ reduction. Treatment of a cold toluene solution of each metal chloride complex with 1 equiv of sodium triethylborohydride led to the formation of the corresponding hydride complexes (Scheme 4; M = Ni (**3-Ni**), Pd (**3-Pd**), Pt (**3-Pt**)). Unlike the related complex (Cy-PSiP)NiH which is thermally sensitive,¹⁴ **3-Ni** does not appear to decompose in solution at temperatures up to 80 °C, as indicated by ¹H and ³¹P NMR analysis.

While the ³¹P and ¹³C NMR spectroscopic features of these hydride complexes are generally similar to those of the chloride precursors, the ¹H and ²⁹Si NMR data are intriguing (Table 1). In particular, the ¹H NMR spectra of **3-Pd** and **3-Pt** (benzene-*d*₆) feature metal hydride resonances at 0.15 ppm (*J*_{PH} = 15 Hz)

Scheme 4. Synthesis of (*i*Pr-PSiP^{Ind})MH (M = Ni, Pd, Pt) ComplexesTable 1. Selected NMR Spectroscopic Data for Group 10 Complexes Supported by ¹Pr-PSiP^{Ind} Ligations^a

compound	¹ H NMR M-H (ppm)	²⁹ Si NMR (ppm)	<i>J</i> _{SiH} (Hz)
3-Ni	-4.79	59.8	n/a
3-Ni*	-2.92 ^b	-10.5 ^b	89 ^{b,c}
3-Pd	0.15	60.1	-101
3-Pt	4.23	64.1	-67
4	-3.50	-24.1	-69
5a	-5.44	6.3	-82
5b	-10.18	65.7	-81

^aConditions unless specified otherwise: benzene-*d*₆, room temperature. ^bToluene-*d*₈, -80 °C. ^cThe sign of *J*_{SiH} could not be determined.

and 4.23 ppm (*J*_{PH} = 18 Hz, *J*_{PH} = 900 Hz), respectively. The latter resonance in particular is atypical for a late-transition-metal hydride, as such resonances are most commonly observed upfield of 0 ppm.¹⁵ By comparison, while the ²⁹Si NMR chemical shifts of these hydride species are not unusual for transition-metal silyls, the large *J*_{SiH} coupling constants

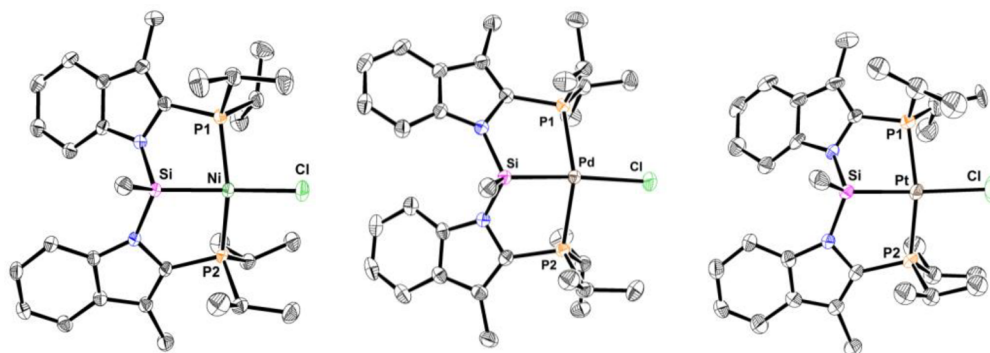


Figure 2. Crystallographically determined structures of **2-Ni**, **2-Pd**, and **2-Pt** with thermal ellipsoids shown at the 50% probability level. Hydrogen atoms have been omitted for clarity. Selected interatomic distances (Å) and angles (deg): **2-Ni**, Ni-Cl 2.2170(5), Ni-P(1) 2.1938(5), Ni-P(2) 2.1824(5), Ni-Si 2.1850(5), Cl-Ni-P(1) 96.58(2), Cl-Ni-P(2) 98.55(2), Cl-Ni-Si 167.82(2), P(1)-Ni-P(2) 154.54(2), P(1)-Ni-Si 83.542(18), P(2)-Ni-Si 85.881(18); **2-Pd**, Pd-Cl 2.4255(5), Pd-P(1) 2.3156(4), Pd-P(2) 2.3216(4), Pd-Si 2.2483(5), Cl-Pd-P(1) 100.407(16), Cl-Pd-P(2) 95.083(16), Cl-Pd-Si 174.176(17), P(1)-Pd-P(2) 159.013(16), P(1)-Pd-Si 84.817(16), P(2)-Pd-Si 81.387(16); **2-Pt**, Pt-Cl 2.432(3), Pt-P(1) 2.311(3), Pt-P(2) 2.283(3), Pt-Si 2.266(3), Cl-Pt-P(1) 94.76(12), Cl-Pt-P(2) 96.84(11), Cl-Pt-Si 175.29(13), P(1)-Pt-P(2) 159.88(10), P(1)-Pt-Si 83.67(9), P(2)-Pt-Si 85.95(9).

observed for **3-Pd** (101 Hz) and **3-Pt** (67 Hz) are intermediate in magnitude between those anticipated for a one-bond J_{SiH} (typical range of ca. 150–200 Hz;¹⁶ cf. $^1J_{\text{SiH}} = 252$ Hz for **1a**) and a two-bond J_{SiH} (≤ 20 Hz).¹⁶ The magnitude of these J_{SiH} constants does not vary as a function of temperature (less than 2 Hz variation in the range of -80 to 60 °C), nor do we observe any other evidence of temperature dependence in the ^1H , ^{29}Si , and ^{31}P NMR features of **3-Pd** and **3-Pt** over this temperature range (toluene- d_8).

In an effort to gain further information regarding Si–H coupling constants for **3-Pd** and **3-Pt**, we also sought to determine the relative sign of the measured J_{SiH} by use of a ^1H – ^{29}Si HECAD E NMR experiment,¹⁷ wherein the $^2J_{\text{SiH}}$ constant for the Si–Me group in the ligand backbone was used as a reference (Figure S8 in the Supporting Information). While $^2J_{\text{SiH}}$ constants are often positive, $^1J_{\text{SiH}}$ constants are known to be negative.¹⁶ Indeed, for **1** the $^1J_{\text{SiH}}$ constant was found to be opposite in sign to the $^2J_{\text{SiH}}$ constant associated with the Si–Me protons, which is consistent with the latter being positive. In the cases of **3-Pd** and **3-Pt** the J_{SiH} constant involving the metal hydride was observed to also be opposite in sign to the $^2J_{\text{SiH}}$ of the Si–Me protons, suggesting that the J_{SiH} constants involving the Pd and Pt hydrides are negative.

Unlike our observations for **3-Pd** and **3-Pt**, the NMR spectroscopic features of **3-Ni** were found to exhibit significant temperature dependence (Figure 3). While the $^{31}\text{P}\{^1\text{H}\}$ NMR spectrum of **3-Ni** features a sharp resonance at 65.6 ppm, the ^1H NMR spectrum of this complex (benzene- d_6) features a broad hydride resonance at -4.80 ppm. At low temperature (-60 °C, toluene- d_8) the latter resonance is resolved into an apparent triplet with $^2J_{\text{PH}} = 47$ Hz. Concurrent with these line-shape changes, low-temperature NMR spectra (^1H , ^{31}P , ^{29}Si)

for **3-Ni** also indicate the presence of a second ($^i\text{Pr-PSiP}^{\text{Ind}}\text{NiH}$) species (**3-Ni***), which appears to interconvert with **3-Ni**. Complex **3-Ni*** gives rise to a ^{31}P NMR resonance at 35.3 ppm and features a hydride ^1H NMR resonance at -2.55 ppm ($^2J_{\text{PH}} = 38$ Hz; toluene- d_8). Below -40 °C the ^{31}P NMR resonance for **3-Ni*** begins to decoalesce, such that at -80 °C it has decoalesced into two broad signals centered at 40.7 and 28.3 ppm, respectively. No such line-shape changes were observed for the ^{31}P NMR resonance corresponding to **3-Ni**, which persists in solution over this temperature range. Interestingly, while **3-Ni** gives rise to a ^{29}Si NMR resonance at 59.8 ppm, the ^{29}Si resonance for **3-Ni*** was observed at -10.5 ppm (-80 °C, toluene- d_8 , $J_{\text{SiH}} = 89$ Hz). Despite repeated efforts, we were unable to determine the sign of the J_{SiH} constant observed for **3-Ni***, nor could we measure the magnitude of J_{SiH} for **3-Ni**, including at low temperature.

The relative ratio of **3-Ni** to **3-Ni*** appears to be both temperature and solvent dependent. As such, while the room-temperature NMR spectra (^1H , ^{31}P , ^{29}Si) of **3-Ni** in benzene- d_6 show no evidence of a second hydride species in solution, a **3-Ni**:**3-Ni*** ratio of ca. 4:1 was observed for a room-temperature toluene- d_8 solution (by ^1H and ^{31}P NMR). When the temperature is decreased to -20 °C, the amount of **3-Ni*** increases to afford a ca. 4:3 ratio of **3-Ni** to **3-Ni***, and a ratio of ca. 1:1 was observed at -80 °C. Somewhat similar behavior was observed when low-temperature NMR data were collected on a sample of **3-Ni** in methylcyclohexane- d_{14} solution (Figure S6 in the Supporting Information). At 20 °C a **3-Ni**:**3-Ni*** ratio of ca. 7:1 was observed (^1H and ^{31}P NMR). This ratio decreased dramatically to 1:1 at 0 °C and decreased further to 1:10 at -20 °C. At -40 °C essentially only **3-Ni*** is present in solution, and the $^{31}\text{P}\{^1\text{H}\}$ NMR signal for this complex is significantly broadened. At -80 °C the $^{31}\text{P}\{^1\text{H}\}$ NMR resonance for **3-Ni*** has decoalesced to two broad signals at 39.8 and 28.0 ppm, respectively. Finally, a degassed toluene- d_8 solution of **3-Ni** showed only negligible formation of **3-Ni***, including at low temperature. This is consistent with a formulation for **3-Ni*** that involves the coordination of N_2 from the reaction atmosphere (Scheme 5).

In considering the formulation of **3-Ni**, **3-Pd**, and **3-Pt** in solution, the NMR features observed (vide supra) suggest several possibilities along the continuum between terminal

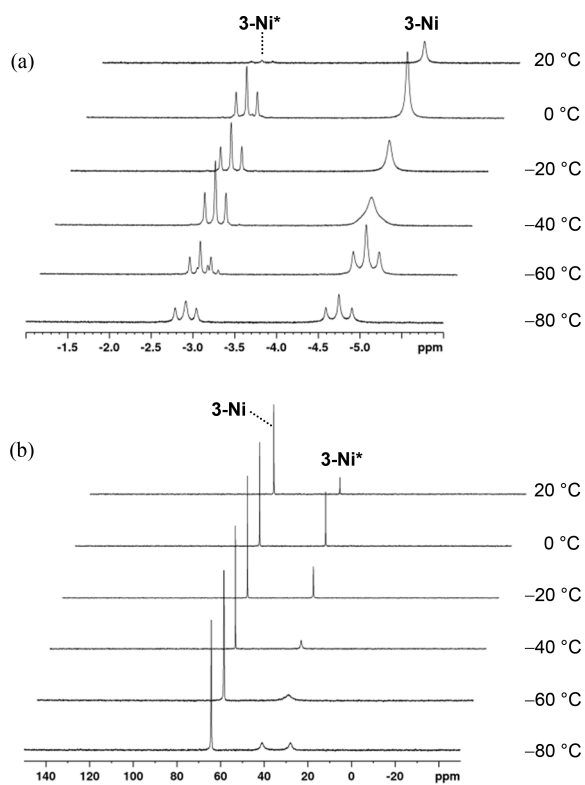
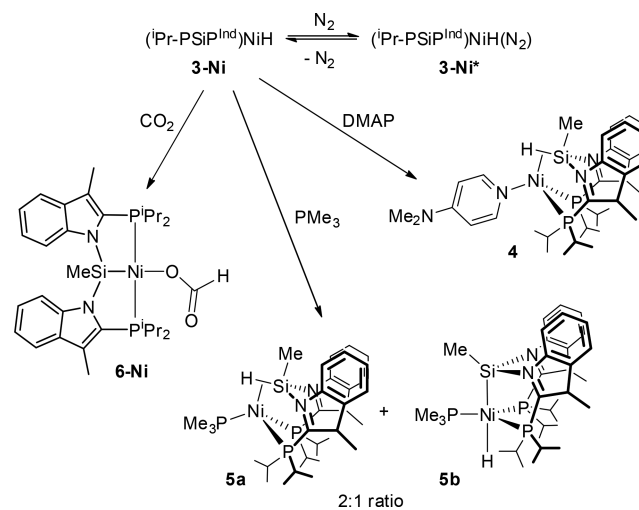


Figure 3. Variable-temperature (a) ^1H NMR (hydride region) and (b) $^{31}\text{P}\{^1\text{H}\}$ NMR spectra of **3-Ni** (toluene- d_8).

Scheme 5. Reactivity of ($^i\text{Pr-PSiP}^{\text{Ind}}\text{NiH}$)



$M^{\text{II}}\text{-H}$ and $(\eta^2\text{-SiH})\text{-M}^0$ complexes (Scheme 4), including scenarios where such species are in equilibrium.^{18,19} For **3-Pd** and **3-Pt**, while no evidence of such an equilibrium process was obtained, the large negative J_{SiH} constants observed for the hydride ligand are in keeping with a scenario where Si–H bonding interactions are non-negligible.^{16,20} On the other hand, the downfield ^{29}Si NMR chemical shifts for these complexes are more typical of transition-metal silyl complexes rather than $(\eta^2\text{-SiH})\text{-M}$ species.¹³ It is thus possible that the observed phenomenon involving the J_{SiH} constants could result from the trans disposition of the hydride and silyl groups in **3-Pd** and **3-Pt**.²¹ While similar trends in ^1H and ^{29}Si NMR data were noted for related PSiP Pt and Pd hydride complexes supported by $\kappa^3\text{-}(2\text{-Cy}_2\text{PC}_6\text{H}_4)_2\text{SiMe}$ ligation,^{7c,13b} the *solid-state* structure of $(\text{Cy-PSiP})\text{PtH}$ has been confirmed to involve terminal Pt–H coordination by neutron diffraction analysis.²¹ With respect to **3-Ni**, ^1H , ^{31}P , and ^{29}Si NMR data provide clear evidence for a temperature- and solvent-dependent equilibrium between two Ni hydride species in solution. Moreover, the Ni hydride species **3-Ni*** that appears to increase in concentration at low temperature involves the coordination of N_2 from the reaction atmosphere (*vide supra*) and gives rise to a significantly upfield shifted ^{29}Si NMR resonance relative to **3-Ni**, **3-Pd**, and **3-Pt**. On the basis of these data, we tentatively assign **3-Ni** as a terminal Ni–H species formulated as $(^i\text{Pr-PSiP}^{\text{Ind}})\text{NiH}$ and **3-Ni*** as an N_2 adduct involving $(\eta^2\text{-SiH})\text{-Ni}$ coordination. The interconversion between such structures in $(\text{Cy-PSiP})\text{NiH(L)}$ ($\text{L} = \text{N}_2, \text{CO}$) has been observed previously, and trends in ^{29}Si NMR data reported for such species are indeed consistent with our observations for **3-Ni** and **3-Ni***.^{18c} On the basis of the NMR data available for **3-Ni***, we cannot definitively determine whether in solution this complex is a monomeric species of the type $[\text{Pr-P}(\eta^2\text{-SiH})\text{P}^{\text{Ind}}]\text{Ni}(\text{N}_2)$ or a related N_2 -bridged dimer. However, in the solid state, the IR spectrum of the Ni hydride features a weak-intensity band at 2075 cm^{-1} while the Raman spectrum features a relatively intense band at 2073 cm^{-1} , which is assigned to coordinated N_2 . These data suggest that in the solid state the Ni hydride is likely best formulated as the N_2 -bridged dimer $\{[\text{Pr-P}(\eta^2\text{-SiH})\text{P}^{\text{Ind}}]\text{Ni}\}_2(\mu\text{-N}_2)$, which would be anticipated to feature a Raman-active N_2 ligand. This result is in agreement with the observations of Hazari and co-workers in regard to the formulation of the related N_2 adducts of $(\text{Cy-PSiP})\text{NiH}$.^{18c}

To investigate further the influence of an added donor ligand on **3-Ni**, the synthesis of complexes of the type $(^i\text{Pr-PSiP}^{\text{Ind}})\text{NiH(L)}$ (Scheme 5; **4**, $\text{L} = \text{DMAP}$; **5**, $\text{L} = \text{PMe}_3$) was pursued. Complexes **4** and **5** were both prepared by treatment of **3-Ni** with 1 equiv of DMAP and PMe_3 , respectively. In the case of **4**, the NMR spectroscopic data obtained (e.g., ^{29}Si chemical shift of -24.1 ppm , $J_{\text{SiH}} = -69\text{ Hz}$) are closely aligned to those of **3-Ni*** and support the formulation of this complex as $[\text{Pr-P}(\eta^2\text{-SiH})\text{P}^{\text{Ind}}]\text{Ni}(\text{DMAP})$ in solution. Indeed, the solid-state structure of **4** determined by X-ray crystallographic analysis is also in agreement with this assignment (Figure 4).

By comparison, in the case of **5**, NMR analysis is consistent with the existence of two Ni hydride species in solution in a ca. 2:1 ratio (**5a**, major; **5b**, minor). While the ^{29}Si chemical shift of 6.3 ppm ($J_{\text{SiH}} = -82\text{ Hz}$) for **5a** is relatively upfield, the minor constituent **5b** gives rise to a ^{29}Si NMR resonance at 65.7 ppm ($J_{\text{SiH}} = -81\text{ Hz}$), which is more closely aligned with NMR data obtained for **3-Ni**. Complexes **5a** and **5b** both exhibit equivalent phosphorus environments associated with the $^i\text{Pr-}$

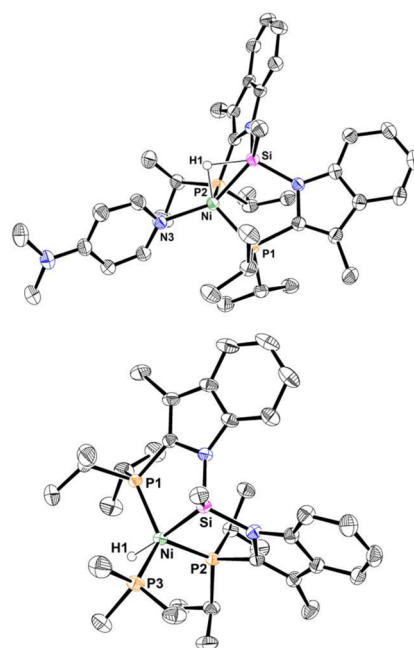


Figure 4. Crystallographically determined structures of **4** and **5b** with thermal ellipsoids drawn at the 50% probability level. Solvent molecules and most hydrogen atoms have been omitted for clarity. Only one of the two crystallographically independent molecules of **4** is shown. Selected interatomic distances (Å) and angles (deg): **4**, Ni–H(1) 1.50(3), Ni–P(1) 2.1816(7), Ni–P(2) 2.2245(8), Ni–Si 2.1745(8), Ni–N(3) 2.040(2), P(1)–Ni–P(2) 118.44(3), P(1)–Ni–Si 89.98(3), P(1)–Ni–N(3) 106.67(7), P(2)–Ni–Si 88.42(3), P(2)–Ni–N(3) 112.97(7), Si–Ni–H(1) 48.3(12), Si–Ni–N(3) 139.99(7), N(3)–Ni–H(1) 93.7(12); **5b**, Ni–H1 1.49(3), Ni–P(1) 2.1611(5), Ni–P(2) 2.1794(5), Ni–P(3) 2.1727(5), Ni–Si 2.2057(5), Si–Ni–H1 175.6(10), P(1)–Ni–P(2) 119.10(2), P(1)–Ni–P(3) 126.58(2), P(1)–Ni–Si 88.024(19), P(1)–Ni–H(1) 87.9(10), P(2)–Ni–P(3) 114.30(2), P(2)–Ni–Si 86.527(19), P(2)–Ni–H(1) 94.1(10), P(3)–Ni–Si 96.89(2), P(3)–Ni–H(1) 86.8(10).

PSiP^{Ind} ligand, which is consistent with C_s -symmetric structures in solution. However, the substantial difference in $^2J_{\text{PP}}$ values for these two complexes ($^2J_{\text{PP}}$ for **5a** 6 Hz; $^2J_{\text{PP}}$ for **5b** 111 Hz) suggests that the orientation of the PMe_3 ligand relative to the $^i\text{Pr-PSiP}^{\text{Ind}}$ phosphino donors is different in each case. The ^{29}Si and ^{31}P NMR data for **5a** are consistent with data previously reported for the related complexes $[\text{Ph-P}(\eta^2\text{-SiH})\text{P}]\text{Ni}(\text{PR}_3)$ ($\text{R} = \text{Ph}, \text{Me}$; $\text{Ph-PSiP} = \kappa^3\text{-}(2\text{-Ph}_2\text{PC}_6\text{H}_4)_2\text{SiMe}$)^{18b,22} that were found to exhibit similarly upfield shifted ^{29}Si NMR resonances, large values of J_{SiH} , and small values of $^2J_{\text{PP}}$. By comparison, NMR data for **5b** are similar to those reported for the trigonal-bipyramidal complex $(\text{Ph-PSiP})\text{PtH}(\text{PPh}_3)$ that features a terminal hydride ligand coordinated trans to Si.^{18b} On the basis of these data, we assign **5a** as a PMe_3 adduct featuring $\eta^2\text{-SiH}$ coordination, while **5b** is assigned as a complex of the type $(^i\text{Pr-PSiP}^{\text{Ind}})\text{NiH}(\text{PMe}_3)$ with a terminal hydride ligand coordinated trans to Si. Thus, it appears the mixture of **5a** and **5b** generated upon treatment of **3-Ni** with PMe_3 represents a unique example of the Si–H oxidative addition product (**5b**) and the $\eta^2\text{-SiH}$ complex associated with “arrested oxidative addition” (**5a**) existing simultaneously in solution as an isomeric mixture. No conclusive evidence for a temperature-dependent equilibrium involving **5a** and **5b** was obtained by ^1H and ^{31}P NMR analysis ($-80\text{--}80\text{ }^\circ\text{C}$), although broadening of NMR features was observed at low temperature and slight

changes in the ratio of **5a** to **5b** were noted at elevated temperatures. In addition, no evidence for chemical exchange was obtained by selective excitation of the NiH resonances via NOESY experiments (0.5 and 1 s mixing times; 80 °C). While we were not able to separate **5a** and **5b** on a preparative scale, a sample of X-ray-quality crystals obtained from the **5a/5b** mixture revealed a five-coordinate complex featuring an approximate trigonal-bipyramidal coordination geometry at Ni with Si and a terminal hydride ligand (H(1)) in the axial positions, which is consistent with our formulation of **5b** (Figure 4). Thus, it appears that a substantial amount of structural variability is possible for (ⁱPr-PSiP^{Ind})NiH(L) complexes, where terminal hydride as well as complexes involving η²-SiH coordination are both accessible and may even coexist, in ratios dependent on factors such as the nature of L, as well as solvent and temperature. Furthermore, on comparison of the NMR features of such bis(phosphino)silyl group 10 hydride complexes (Table 1), the available data suggest that such species generally feature relatively large, negative *J*_{SiH} values that can be associated with both η²-SiH interactions and *trans*-Si–M–H coordination. Indeed, the NMR data obtained appear to suggest that in this specific family of complexes the ²⁹Si chemical shift may be a better predictor of the extent of Si–H interaction, such that complexes that feature an η²-SiH interaction involving the ⁱPr-PSiP^{Ind} ligand also give rise to relatively upfield shifted ²⁹Si NMR resonances (Table 1).

To probe the ability of such group 10 hydride species to reduce CO₂, **3-Ni** was treated with ca. 1 atm CO₂ (benzene-*d*₆), which led to the quantitative generation of the Ni formate complex **6-Ni** (Scheme 5). While **6-Ni** appears to decompose upon attempted isolation, this complex was characterized in situ spectroscopically. The ¹H NMR spectrum of **6-Ni** features a characteristic singlet resonance at 8.71 ppm that corresponds to the formate proton. This resonance correlates to a ¹³C NMR resonance at 168.8 ppm in a ¹H–¹³C HSQC experiment, which is assigned to the carbonyl of the formate ligand. The ³¹P{¹H} NMR spectrum of **6-Ni** features a singlet resonance at 34.6 ppm, which is consistent with its formulation as a C_s-symmetric complex. Finally, the ²⁹Si NMR spectrum of **6-Ni** features a resonance at 42.2 ppm. These data are in agreement with those reported for the related Ni formate complex (Cy-PSiP)Ni(HCO₂).¹⁴

In the case of Pd, treatment of **3-Pd** with CO₂ (ca. 1 atm, benzene-*d*₆) also appears to generate a formate complex (**6-Pd**) as the major product; however, this reaction is not as clean as in the case of Ni and **6-Pd** could not be successfully isolated. ¹H NMR analysis of the reaction mixture indicates that **6-Pd** gives rise to a formate resonance at 9.26 ppm. Attempts to generate an analogous Pt formate species by treatment of **3-Pt** with CO₂ led to the formation of multiple unidentified products from which no pure material could be isolated. By comparison, the related Pd formate complex (Cy-PSiP)Pd(HCO₂) is isolable, while the Pt derivative can be generated under a CO₂ atmosphere and readily eliminates CO₂ to reform the parent Pt hydride complex.^{7c}

Catalytic Hydroboration of CO₂. Having observed facile insertion of CO₂ by **3-Ni** to afford a Ni formate complex, we focused our attention on the development of catalytic CO₂ reduction chemistry mediated by such hydride complexes. Catalytic reactions were carried out in benzene solution at room temperature and 1 atm of CO₂, with HBPIn as the reductant. In an initial screen, the catalytic performances of **3-**

Ni, **3-Pd**, and **3-Pt**, respectively, were assessed (Table 2). After a 1 h reaction time, NMR analysis of the reaction mixtures

Table 2. Hydroboration of CO₂ with HBPIn^a

entry	catalyst	conversion (%)		
		7-A	7-B	7-C
1	3-Ni	<5	84 (1.8 mmol) ^b	<5
2	3-Pd	39 (1.6 mmol)	6	<5
3	3-Pt	<5	<5	<5
4	2-Ni	0	0	0
5	NaEt ₃ BH	0	0	0

^aReaction conditions: benzene-*d*₆, 4.2 mmol of HBPIn, [HBPIn] = 4.8 M, 1 atm of CO₂, 0.2 mol % of M (M = Ni, Pd, Pt) or NaEt₃BH vs HBPIn, room temperature, 1 h. Conversions were determined on the basis of ¹H NMR integration using C₆Me₆ as an internal standard (average of two runs). ^bTON = 420 based on moles of B–H reacted per mole of Ni.

indicated negligible formation of products resulting from CO₂ hydroboration in the case of **3-Pt**. For **3-Pd**, 39% conversion to PinB(CO₂H) (**7-A**) was observed, with minimal formation of other hydroboration products (Table 2, entry 2). By comparison, for **3-Ni** highly selective formation of the bis(boryl)acetal **7-B** was observed, as indicated by a characteristic ¹H NMR resonance at 5.51 ppm corresponding to the methylene protons of the acetal.^{6a} In an effort to establish the necessity of **3-Ni** for this reactivity, control experiments utilizing **2-Ni** as the Ni source were carried out under identical conditions with no CO₂ reduction products observed spectroscopically after 1 h (Table 2, entry 4). Similarly, NaEt₃BH alone was not effective as a catalyst (Table 2, entry 5).

Intrigued by the selectivity of **3-Ni** for the reduction of CO₂ to the formaldehyde level, we conducted further experiments to optimize this reactivity (Table 3). We first established that, under the initial screening conditions, increasing the reaction

Table 3. Hydroboration of CO₂ with **3-Ni to the Formaldehyde Level^a**

$$2 \text{HBR}_2 + \text{CO}_2 \xrightarrow{\text{3-Ni, RT}} (\text{R}_2\text{BO})_2\text{CH}_2$$

7-B for R₂B = BPIn

entry	Ni (mol %)	HBR ₂	[HBR ₂] (mol/L)	solvent	time (h)	conversion to acetal (%)
1	0.2	HBPIn	4.8	C ₆ D ₆	4	97 ^b
2	0.02	HBPIn	4.8	C ₆ D ₆	1	<5
3	0.2	HBPIn	4.8	C ₆ D ₆	1	84
4	0.2	HBPIn	0.96	C ₆ D ₆	1	21
5	0.2	HBPIn	0.096	C ₆ D ₆	1	<5
6	0.2	HBCat	4.8	C ₆ D ₆	1	<5
7	0.2	9-BBN	0.96	C ₆ D ₆	1	<5
8	0.2	HBPIn	4.8	THF- <i>d</i> ₈	1	30
9	0.2	HBPIn	4.8	C ₆ D ₁₂	1	92

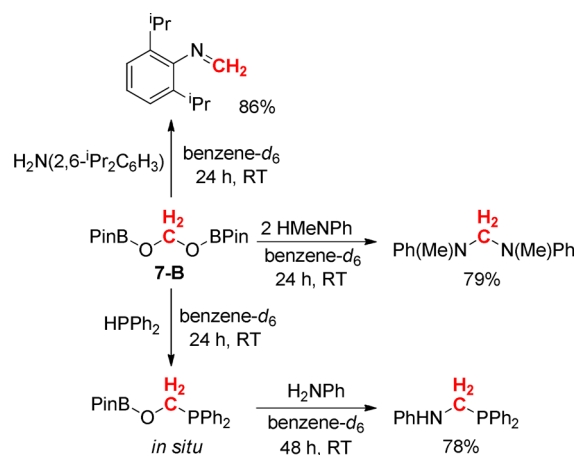
^aUnder 1 atm of CO₂. Conversions were determined on the basis of ¹H NMR integration using C₆Me₆ as an internal standard (average of two runs). Throughout, no indication of boryl formate and minimal (<5%) conversion to methoxyborane were observed. ^bTON = 487 based on moles of B–H reacted per mole of Ni; 71% isolated yield.

time to 4 h led to 97% conversion of HBPIn to the targeted acetal 7-B. This represents the highest selectivity reported to date for hydroboration to the formaldehyde level with negligible overreduction to the methoxyborane 7-C (ca. 1% by ^1H NMR analysis after 4 h).¹⁰ By comparison, in the only previous example of selective CO_2 double hydroboration (with 9-BBN), a yield of 85% bis(boryl)acetal and 8% methoxyborane was obtained at full 9-BBN conversion by use of $\text{Fe}(\text{H})_2(\text{DMPE})_2$ as the precatalyst.^{6c} Decreasing the catalyst loading by a factor of 10 led to a dramatic dropoff in reactivity (Table 3, entry 2). We evaluated the effect of concentration on the catalytic performance of 3-Ni by performing reactions at lower concentrations of HBPIn and once again found that the conversion to the bis(boryl)acetal product decreased significantly (Table 3, entries 4 and 5). We also examined the reactivity of alternative boranes and found that HBCat and 9-BBN each provided negligible conversion to any products arising from CO_2 hydroboration (Table 3, entries 6 and 7). Finally, we explored the effect of varying the solvent by performing the catalytic reaction in $\text{THF}-d_8$ and cyclohexane- d_{12} solution and found that while the use of THF resulted in decreased formation of the bis(boryl)acetal product, the use of cyclohexane resulted in 92% conversion to 7-B in 1 h at room temperature (Table 3, entries 8 and 9).

Having optimized reaction conditions for the formation of 7-B, we also found that this compound could be readily isolated as an analytically pure, moisture-sensitive solid in 71% yield, which may facilitate its utility as a synthon for subsequent chemical manipulation. Samples of 7-B stored under a nitrogen atmosphere proved stable in the solid state for several days. While 7-B rapidly hydrolyzes to generate formaldehyde upon exposure to water, in benzene- d_6 solution under an inert atmosphere 64% of the acetal was found to persist after 96 h at room temperature (by ^1H NMR integration relative to ferrocene internal standard).

Bontemps, Sabo-Etienne, and co-workers have previously reported that in situ generated bis(boryl)acetal derived from the hydroboration of CO_2 with 9-BBN is an effective source of formaldehyde that can undergo subsequent reactivity with substrates such as anilines, amines, alcohols, and ylides to form C–N, C–O, and C–C bonds.^{6e,23} Intrigued by this reactivity, we sought to study the reactivity of isolated 7-B in this regard. Indeed, similar methylene transfer reactivity was observed for the reaction of 7-B with anilines (Scheme 6), such that

Scheme 6. Methylene Transfer from 7-B



treatment with $\text{H}_2\text{N}(2,6\text{-iPr}_2\text{C}_6\text{H}_3)$ led to the formation of $\text{CH}_2=\text{N}(2,6\text{-iPr}_2\text{C}_6\text{H}_3)$ (86% conversion by ^1H NMR after 24 h at room temperature), while treatment with HMeNPh led to the formation of $[\text{Ph}(\text{Me})\text{N}]_2\text{CH}_2$ (79% conversion after 24 h at room temperature). We also observed net methylene transfer to phosphorus upon treatment of 7-B with HPPH_2 . While the latter reaction leads exclusively to the generation of a monophosphine intermediate, which we tentatively assign as $\text{PinBOCH}_2\text{PPh}_2$, treatment of this species (generated in situ) with H_2NPh led to the formation of $\text{Ph}(\text{H})\text{NCH}_2\text{PPh}_2$ (78% based on 7-B). This reactivity confirms the utility of 7-B as an effective methylene transfer reagent.

CONCLUSION

In summary, a new bis(indolylphosphino)silyl PSiP ligand was developed and utilized for the synthesis of group 10 pincer complexes. Nickel, palladium, and platinum hydride complexes supported by this ligand were prepared and characterized. Solution NMR and single-crystal X-ray data revealed that a significant amount of structural variability is possible for such complexes, particularly in the case of Ni, where terminal hydride as well as complexes involving $\eta^2\text{-SiH}$ coordination are both accessible and may even coexist, in ratios dependent on factors such as the nature of additional coligands, including N_2 from the reaction atmosphere, as well as solvent and temperature.

While both the Ni and Pd hydride complexes were shown to be capable of CO_2 insertion to afford formate complexes, these formate complexes were not isolable. However, both hydride species were active for catalytic hydroboration of CO_2 with HBPIn, displaying divergent selectivity. Thus, the Pd catalyst exhibited moderate activity in the hydroboration of CO_2 to the formate level, whereas the analogous Ni species exhibited unprecedented selectivity for hydroboration to the formaldehyde level. We further demonstrated that the HBPIn-derived bis(boryl)acetal product could be successfully isolated and utilized as a source of methylene for the formation of C–N and C–P bonds.

EXPERIMENTAL SECTION

General Considerations. All experiments were conducted under N_2 in a glovebox or using standard Schlenk techniques. Tetrahydrofuran and diethyl ether were distilled from Na/benzophenone ketyl. Benzene, toluene, and pentane were first sparged with nitrogen and subsequently dried by passage through a double-column (one activated alumina column and one column packed with activated Q-5) solvent purification system. All purified solvents were stored over 4 Å molecular sieves. Deuterated solvents were degassed via three freeze–pump–thaw cycles and stored over 4 Å molecular sieves. All reagents were purchased from commercial suppliers and used without further purification. The compound diisopropyl(3-methyl-2-indolyl)phosphine was prepared according to a literature procedure.¹² Unless otherwise stated, ^1H , ^{13}C , ^{11}B , ^{31}P , and ^{29}Si characterization data were collected at 300 K, with chemical shifts reported in parts per million downfield of SiMe_4 (for ^1H , ^{13}C , and ^{29}Si), $\text{BF}_3\cdot\text{OEt}_2$ (for ^{11}B), or 85% H_3PO_4 in D_2O (for ^{31}P). Chemical shift ranges are cited to indicate overlapping resonances. ^1H and ^{13}C NMR chemical shift assignments are based on data obtained from $^{13}\text{C}\{^1\text{H}\}$, ^{13}C -DEPTQ, ^1H - ^1H COSY, ^1H - ^{13}C HSQC, and ^1H - ^{13}C HMBC NMR experiments. ^{29}Si NMR assignments are based on ^1H - ^{29}Si HMBC, ^1H - ^{29}Si HMQC, and ^1H - ^{29}Si HECAD¹⁷ experiments. The 2D ^1H - ^{29}Si HECAD data were acquired using a value for the one-bond ^1H - ^{29}Si coupling of 180 Hz and a TOCSY mixing time of 60 ms; in order to ensure adequate digital resolution in F2 for the measurement of coupling constants, the acquisition time was adjusted to 1.14 s, resulting in a

digital resolution of 0.88 Hz/point. In experiments involving the reactivity of the acetal **7-B**, a 60 s relaxation delay was used when determining reaction yields by NMR integration relative to a ferrocene internal standard. Infrared spectra were recorded as thin films between NaCl plates at a resolution of 4 cm⁻¹. Raman spectroscopy was performed using a DXR Smart Raman Spectrometer. Elemental analyses were performed by Canadian Microanalytical Service Ltd. of Delta, British Columbia, Canada, or Galbraith Laboratories Inc. of Knoxville, TN, USA.

(Pr-PSiP^{Ind})H (1). A precooled (-78 °C) solution of diisopropyl(3-methyl-2-indolyl)phosphine (4.00 g, 16.2 mmol) in THF (ca. 100 mL) was treated with ⁿBuLi (1.6 M in hexanes, 10.1 mL, 16.2 mmol), added dropwise over the course of 10 min. The resulting reaction mixture was stirred for 20 min at -78 °C and then warmed to room temperature over the course of 1 h. The reaction mixture was once again cooled to -78 °C, and neat Cl₂SiHMe (0.84 mL, 8.10 mmol) was added by syringe. The mixture was warmed to room temperature over the course of 18 h with stirring, during which time a white precipitate was observed. The volatile components of the reaction mixture were subsequently removed under vacuum, and benzene (ca. 60 mL) was added to the remaining residue. The resulting slurry was filtered through Celite. The filtrate solution was collected, and the volatile components were removed in vacuo. The remaining residue was triturated with pentane (4 × 3 mL) and subsequently washed with pentane (3 × 4 mL) to afford **1a** (3.21 g, 74% yield) as an off-white solid. ¹H NMR (500 MHz, benzene-*d*₆): δ 7.56 (apparent d, 4 H, *J* = 8 Hz, *H*_{arom}), 7.25–7.09 (5 H, SiH + *H*_{arom}; the SiH resonance was identified at 7.19 ppm by the use of ¹H–²⁹Si correlation spectroscopy), 2.27 (s, 6 H, Indole-Me), 2.22 (m, 4 H, PCHMe₂), 1.19 (m, 3 H, SiMe), 1.04 (dd, 6 H, ³*J*_{HH} = 7 Hz, ³*J*_{HP} = 16 Hz, PCHMe₂), 0.98 (dd, 6 H, ³*J*_{HH} = 7 Hz, ³*J*_{HP} = 17 Hz, PCHMe₂), 0.77 (dd, 6 H, ³*J*_{HH} = 7 Hz, ³*J*_{HP} = 13 Hz, PCHMe₂), 0.67 (dd, 6 H, ³*J*_{HH} = 7 Hz, ³*J*_{HP} = 14 Hz, PCHMe₂). ¹³C{¹H} NMR (126 MHz, benzene-*d*₆): δ 143.3 (*C*_{arom}), 136.1 (*C*_{arom}), 133.4 (*C*_{arom}), 123.2 (CH_{arom}), 120.5 (CH_{arom}), 118.9 (CH_{arom}), 115.5 (CH_{arom}), 25.9 (apparent d, *J* = 9 Hz, PCHMe₂), 25.2 (apparent d, *J* = 9 Hz, PCHMe₂), 22.1–21.4 (overlapping resonances, PCHMe₂), 11.1 (Indole-Me), 4.5 (SiMe). ³¹P{¹H} NMR (202 MHz, benzene-*d*₆): δ -8.5. ²⁹Si NMR (100 MHz, benzene-*d*₆): δ -27.3 (*J*_{SiH} = -271 Hz). Anal. Calcd for C₃₁H₄₆N₂P₂Si: C, 69.37; H, 8.64; N, 5.22. Found: C, 69.47; H, 8.89; N, 5.25.}}}}}}}}}

(Pr-PSiP^{Ind})NiCl (2-Ni). A room-temperature solution of **1** (0.40 g, 0.75 mmol) in benzene (ca. 3 mL) was added to a suspension of NiCl₂(DME) (0.16 g, 0.75 mmol) in benzene (ca. 3 mL). Neat NEt₃ (1.05 mL, 7.5 mmol) was added, and the resulting mixture was stirred for 16 h at room temperature. The reaction mixture was subsequently filtered through Celite. The filtrate solution was collected, and the volatile components were removed under vacuum. The remaining residue was triturated with pentane (3 × 5 mL) and then washed with pentane (ca. 1 mL) and dried under vacuum to afford **2-Ni** (0.43 g, 91% yield) as an orange-yellow solid. ¹H NMR (300 MHz, benzene-*d*₆): δ 7.64 (m, 2 H, *H*_{arom}), 7.57 (m, 2 H, *H*_{arom}), 7.21–7.15 (4 H, *H*_{arom}), 2.95 (m, 2 H, PCHMe₂), 2.72 (m, 2 H, PCHMe₂), 2.24 (s, 6 H, Indole-Me), 1.48 (m, 12 H, PCHMe₂), 1.18–1.04 (12 H, PCHMe₂), 0.54 (s, 3 H, SiMe). ¹³C NMR (75.5 MHz, benzene-*d*₆): δ 141.6 (apparent t, *J* = 6 Hz, *C*_{arom}), 138.0 (*C*_{arom}), 133.2 (apparent t, *J* = 27 Hz, *C*_{arom}), 123.8 (CH_{arom}), 121.6 (CH_{arom}), 120.9 (*C*_{arom}), 120.4 (CH_{arom}), 117.5 (CH_{arom}), 28.7 (apparent t, *J* = 12 Hz, PCHMe₂), 27.5 (apparent t, *J* = 13 Hz, PCHMe₂), 20.8 (apparent d, *J* = 12 Hz, CHMe₂), 20.3 (apparent d, *J* = 11 Hz, CHMe₂), 12.2 (Indole-Me), 6.4 (SiMe). ³¹P{¹H} NMR (121.5 MHz, benzene-*d*₆): δ 36.0. ²⁹Si NMR (59.6 MHz, benzene-*d*₆): δ 43.8. Anal. Calcd for C₃₁H₄₅ClN₂P₂NiSi: C, 59.11; H, 7.20; N, 4.45. Found: C, 59.58; H, 7.19; N, 4.12. Although these results in % C are outside the range viewed as establishing analytical purity, they are provided to illustrate the best values obtained to date. Crystals of **2-Ni** suitable for X-ray diffraction analysis were obtained from a concentrated Et₂O solution at -35 °C.

(Pr-PSiP^{Ind})PdCl (2-Pd). A solution of [(*η*³-C₃H₅)PdCl]₂ (0.085 g, 0.23 mmol) in benzene (ca. 5 mL) was added to a solution of **1** (0.25 g, 0.47 mmol) in benzene (ca. 5 mL). The reaction mixture was stirred

at room temperature for 20 min. The volatile components of the reaction mixture were subsequently removed under vacuum. The remaining residue was triturated with 3 × 2 mL of pentane and then washed with pentane (ca. 1 mL) and dried under vacuum to afford **2-Pd**·C₃H₁₂ (0.31 g, 88% yield) as a white solid. Despite prolonged exposure to vacuum, **2-Pd** as prepared above was found to routinely retain pentane (≤1 equiv). ¹H NMR (300 MHz, benzene-*d*₆): δ 7.62–7.56 (4 H, *H*_{arom}), 7.25–7.11 (4 H, *H*_{arom}), 3.18 (m, 2 H, PCHMe₂), 2.63 (m, 2 H, PCHMe₂), 2.22 (s, 6 H, Indole-Me), 1.56 (m, 6 H, PCHMe₂), 1.42 (m, 6 H, PCHMe₂), 1.09 (m, 6 H, PCHMe₂), 0.96 (m, 6 H, PCHMe₂), 0.54 (s, 3 H, SiMe). ¹³C NMR (75.5 MHz, benzene-*d*₆): δ 141.3 (apparent t, *J* = 7 Hz, *C*_{arom}), 137.4 (*C*_{arom}), 132.3 (apparent t, *J* = 25 Hz, *C*_{arom}), 123.4 (CH_{arom}), 121.6 (*C*_{arom}), 121.2 (CH_{arom}), 119.9 (CH_{arom}), 117.2 (CH_{arom}), 28.7 (apparent t, *J* = 13 Hz, PCHMe₂), 26.7 (apparent t, *J* = 13 Hz, PCHMe₂), 20.4–19.5 (overlapping resonances, PCHMe₂), 11.5 (Indole-Me), 7.0 (SiMe). ³¹P{¹H} NMR (121.5 MHz, benzene-*d*₆): δ 38.5. ²⁹Si NMR (59.6 MHz, benzene-*d*₆): δ 41.8. Anal. Calcd for C₃₁H₄₅ClN₂P₂PdSi·C₃H₁₂ (**2-Pd**·C₃H₁₂): C, 57.67; H, 7.66; N, 3.74. Found: C, 58.00; H, 7.02; N, 3.58. Although these results in % H are outside the range viewed as establishing analytical purity, they are provided to illustrate the best values obtained to date. Crystals of **2-Pd** suitable for X-ray diffraction analysis were grown from a concentrated Et₂O solution at -35 °C.

(Pr-PSiP^{Ind})PtCl (2-Pt). A solution of **1** (0.25 g, 0.47 mmol) in benzene (ca. 5 mL) was added to a solution of (Et₂S)₂PtCl₂ (0.21 g, 0.47 mmol) in benzene (ca. 5 mL). Neat NEt₃ (0.65 mL, 4.7 mmol) was added to the reaction mixture. The solution was subsequently heated at 75 °C with stirring for 4 days, during which time a color change to bright yellow was observed. The reaction mixture was subsequently cooled to room temperature and was filtered through Celite. The filtrate solution was collected, and the volatile components were removed under vacuum. The remaining residue was washed with pentane (2 × 3 mL) and dried under vacuum to afford **2-Pt**·C₃H₁₂ (0.33 g, 84% yield) as an off-white solid. Despite prolonged exposure to vacuum, **2-Pt** as prepared above was found to routinely retain pentane (≤1 equiv); other minor unidentified impurities are also apparent in the ¹H NMR spectrum of **2-Pt** (see Figure S4a in the Supporting Information). ¹H NMR (300 MHz, benzene-*d*₆): δ 7.80 (m, 2 H, *H*_{arom}), 7.58 (m, 2 H, *H*_{arom}), 7.24–7.18 (4 H, *H*_{arom}), 3.45 (m, 2 H, PCHMe₂), 2.84 (m, 2 H, PCHMe₂), 2.24 (s, 6 H, Indole-Me), 1.53 (m, 6 H, PCHMe₂), 1.41 (m, 6 H, PCHMe₂), 1.12 (m, 6 H, PCHMe₂), 0.94 (m, 6 H, PCHMe₂), 0.53 (s with Pt satellites, 3 H, ³*J*_{PtH} = 22 Hz, SiMe). ¹³C NMR (75.5 MHz, benzene-*d*₆): δ 141.2 (*C*_{arom}), 137.4 (*C*_{arom}), 132.3 (apparent t, *J* = 31 Hz, *C*_{arom}), 123.4 (CH_{arom}), 121.4 (*C*_{arom}), 121.1 (CH_{arom}), 120.1 (CH_{arom}), 117.3 (CH_{arom}), 28.0 (apparent t, *J* = 16 Hz, PCHMe₂), 27.0 (apparent t, *J* = 16 Hz, PCHMe₂), 20.1–19.2 (overlapping resonances, PCHMe₂), 11.4 (Indole-Me), 5.2 (SiMe). ³¹P{¹H} NMR (121.5 MHz, benzene-*d*₆): δ 42.0 (s with Pt satellites, ¹*J*_{PtP} = 2719 Hz). ²⁹Si NMR (59.6 MHz, benzene-*d*₆): δ 22.2 (s with Pt satellites, ¹*J*_{SiPt} = 1506 Hz). Anal. Calcd for C₃₁H₄₅ClN₂P₂PtSi·C₃H₁₂ (**2-Pt**·C₃H₁₂): C, 51.57; H, 6.85; N, 3.34. Found: C, 52.37; H, 6.60; N, 3.29. Although these results in % C are outside the range viewed as establishing analytical purity, they are provided to illustrate the best values obtained to date. Crystals of **2-Pt** suitable for X-ray diffraction analysis were obtained from a concentrated Et₂O solution at -35 °C.}}}

(Pr-PSiP^{Ind})NiH (3-Ni). A cold (-35 °C) solution of **2-Ni** (0.10 g, 0.16 mmol) in toluene (ca. 5 mL) was treated with NaEt₃BH (1.0 M in toluene, 0.16 mL, 0.16 mmol), which was added in a dropwise manner via pipet. The resulting yellow solution was warmed to room temperature over the course of 2 h with stirring. The volatile components of the reaction mixture were subsequently removed under vacuum. The remaining residue was triturated with 3 × 2 mL of pentane and then extracted with pentane (ca. 10 mL). The combined extracts were filtered through Celite, and the clear yellow filtrate solution was collected. The filtrate was evaporated to dryness in vacuo, and the remaining residue was subsequently washed with cold (-35 °C) pentane (3 × 0.5 mL) and dried under vacuum to afford a yellow solid, which is formulated as the N₂-bridged dimer {[¹Pr-P(*η*²-SiH)P^{Ind}]Ni₂(μ-N₂)} (0.068 g, 70% yield) on the basis of IR and

Raman analysis. Raman data for isolated $\{[\text{Pr-P}(\eta^2\text{-SiH})\text{P}^{\text{Ind}}]\text{Ni}\}_2(\mu\text{-N}_2)$ (solid state, cm^{-1}): 2073 (s). IR (thin film, cm^{-1}): 2075 (w). Repeated attempts to obtain satisfactory elemental analysis for isolated $\{[\text{Pr-P}(\eta^2\text{-SiH})\text{P}^{\text{Ind}}]\text{Ni}\}_2(\mu\text{-N}_2)$ were unsuccessful.

As discussed in the text (vide supra), upon dissolution in benzene $\{[\text{Pr-P}(\eta^2\text{-SiH})\text{P}^{\text{Ind}}]\text{Ni}\}_2(\mu\text{-N}_2)$ generates **3-Ni** quantitatively (by NMR analysis). NMR data for **3-Ni**: ^1H NMR (300 MHz, benzene- d_6) δ 8.13 (apparent d, 2 H, H_{arom}), 7.63 (m, 2 H, H_{arom}), 7.28–7.18 (4 H, H_{arom}), 2.59 (m, 2 H, PCHMe_2), 2.39 (m, 2 H, PCHMe_2), 2.33 (s, 6 H, Indole-Me), 1.36–1.19 (12 H, PCHMe_2), 1.01 (m, 6 H, PCHMe_2), 0.90 (s, 3 H, SiMe), 0.87–0.77 (6 H, PCHMe_2), –4.79 (br s, 1 H, NiH); ^1H NMR (300 MHz, –60 °C, toluene- d_8) δ –4.91 (br t, $^2J_{\text{PH}} = 47$ Hz, 1 H, NiH); ^{13}C NMR (125.8 MHz, benzene- d_6) δ 141.4 (apparent t, $J = 6$ Hz, C_{arom}), 138.0 (apparent t, $J = 26$ Hz, C_{arom}), 137.3 (C_{arom}), 123.0 (CH_{arom}), 120.2 (CH_{arom}), 119.7 (CH_{arom}), 118.0 (C_{arom}), 116.2 (CH_{arom}), 29.0 (apparent t, $J = 14$ Hz, PCHMe_2), 25.5 (apparent t, $J = 16$ Hz, PCHMe_2), 21.6 (PCHMe_2), 20.9 (PCHMe_2), 19.3 (PCHMe_2), 19.1 (PCHMe_2), 11.2 (Indole-Me), 5.6 (SiMe); $^{31}\text{P}\{^1\text{H}\}$ NMR (121.5 MHz, benzene- d_6) δ 65.6; ^{29}Si NMR (99.4 MHz, benzene- d_6) δ 59.8. Despite repeated efforts, we were unable to measure the value of J_{SiH} for **3-Ni**.

The reversible coordination of N_2 to **3-Ni** in solution is both temperature and solvent dependent, such that formation of the N_2 adduct **3-Ni*** can be observed at low temperature. Selected NMR data for **3-Ni***: ^1H NMR (300 MHz, 0 °C, toluene- d_8) δ –2.92 (t, $^2J_{\text{PH}} = 38$ Hz, 1 H, NiH), a 3:2 ratio of **3-Ni** to **3-Ni*** was observed; ^1H NMR (300 MHz, –40 °C, methylcyclohexane- d_{14}) δ –2.58 (t, $^2J_{\text{PH}} = 38$ Hz, 1 H, NiH), near-quantitative formation of **3-Ni*** was observed; $^{31}\text{P}\{^1\text{H}\}$ NMR (121.5 MHz, 0 °C, toluene- d_8) δ 35.2 (s); $^{31}\text{P}\{^1\text{H}\}$ NMR (121.5 MHz, –80 °C, toluene- d_8) δ 40.7 (br s, 1 P), 27.9 (br s, 1 P); ^{29}Si NMR (99.4 MHz, –80 °C, toluene- d_8) δ –10.5 ($J_{\text{SiH}} = 89$ Hz). Despite repeated efforts, we were unable to measure the sign of J_{SiH} for **3-Ni***.

(Pr-PSiP^{Ind})PdH (3-Pd). A cold (–35 °C) solution of **2-Pd** (0.11 g, 0.16 mmol) in toluene (ca. 10 mL) was treated with NaEt_3BH (1.0 M in toluene, 0.16 mL, 0.16 mmol), which was added in a dropwise manner via pipet. The resulting solution was warmed to room temperature over the course of 18 h with stirring. The volatile components of the reaction mixture were subsequently removed under vacuum, and the remaining residue was triturated with 3×1 mL of pentane. The residue was then extracted with pentane (ca. 10 mL), and the combined extracts were filtered through Celite. The filtrate solution was evaporated to dryness in vacuo, and the remaining residue was washed with cold pentane (3×0.5 mL) and dried under vacuum to afford **3-Pd** (0.086 g, 86% yield) as an orange-yellow solid. ^1H NMR (300 MHz, benzene- d_6): 8.06 (m, 2 H, H_{arom}), 7.63 (m, 2 H, H_{arom}), 7.28–7.17 (4 H, H_{arom}), 2.58 (m, 2 H, PCHMe_2), 2.40 (m, 2 H, PCHMe_2), 2.31 (s, 6 H, Indole-Me), 1.43 (m, 6 H, PCHMe_2), 1.26 (m, 6 H, PCHMe_2), 1.00–0.77 (15 H, PCHMe_2 + SiMe; the SiMe resonance was identified at 0.92 ppm by correlation spectroscopy), 0.15 (br t, $^2J_{\text{PH}} = 15$ Hz, 1 H, PdH). $^{13}\text{C}\{^1\text{H}\}$ NMR (75.5 MHz, benzene- d_6): δ 141.5 (apparent t, $J = 7$ Hz, C_{arom}), 137.7 (apparent t, $J = 26$ Hz, C_{arom}), 137.4 (C_{arom}), 123.0 (CH_{arom}), 120.4 (CH_{arom}), 119.7 (CH_{arom}), 119.0 (C_{arom}), 116.7 (CH_{arom}), 28.6 (apparent t, $J = 14$ Hz, PCHMe_2), 26.2 (apparent t, $J = 14$ Hz, PCHMe_2), 22.3 (PCHMe_2), 20.8 (PCHMe_2), 19.9–19.4 (overlapping resonances, PCHMe_2), 19.6 (PCHMe_2), 11.2 (Indole-Me), 7.0 (SiMe). $^{31}\text{P}\{^1\text{H}\}$ NMR (121.5 MHz, benzene- d_6): δ 63.3. ^{29}Si NMR (99.4 MHz, benzene- d_6): δ 60.1 ($J_{\text{SiH}} = -101$ Hz). Anal. Calcd for $\text{C}_{31}\text{H}_{46}\text{N}_2\text{P}_2\text{PdSi}$: C, 57.89; H, 7.21; N, 4.36. Found: C, 57.52; H, 7.31; N, 4.03.

(Pr-PSiP^{Ind})PtH (3-Pt). A cold (–35 °C) solution of **2-Pt** (0.11 g, 0.14 mmol) in toluene (ca. 10 mL) was treated with NaEt_3BH (1.0 M in toluene, 0.14 mL, 0.14 mmol), which was added in a dropwise manner via pipet. The resulting solution was warmed to room temperature over the course of 18 h with stirring. The volatile components of the reaction mixture were subsequently removed under vacuum, and the remaining residue was triturated with 3×1 mL of pentane. The residue was then extracted with pentane (ca. 10 mL), and the combined extracts were filtered through Celite. The filtrate

was evaporated to dryness in vacuo, and the remaining residue was washed with cold pentane (3×0.5 mL) and dried under vacuum to afford **3-Pt** (C_3H_{12} (0.086 g, 76% yield) as a tan solid. Despite prolonged exposure to vacuum, **3-Pt** as prepared above was found to routinely retain pentane (≤ 1 equiv). ^1H NMR (300 MHz, benzene- d_6): δ 8.17 (apparent d, $J = 8$ Hz, 2 H, H_{arom}), 7.63 (m, 2 H, H_{arom}), 7.31–7.19 (4 H, H_{arom}), 4.21 (t with Pt satellites, $^2J_{\text{PH}} = 18$ Hz, H_{arom}), 2.64 (m, 2 H, PCHMe_2), 2.46 (m, 2 H, PCHMe_2), 2.31 (s, 6 H, Indole-Me), 1.41 (m, 6 H, PCHMe_2), 1.20 (m, 6 H, PCHMe_2), 0.97–0.78 (15 H, PCHMe_2 + SiMe; the SiMe resonance was identified at 0.94 ppm by correlation spectroscopy). ^{13}C NMR (75.5 MHz, benzene- d_6): δ 141.0 (apparent t, $J = 6$ Hz, C_{arom}), 137.5 (C_{arom}), 136.7 (C_{arom}), 122.9 (CH_{arom}), 120.1 (CH_{arom}), 119.8 (CH_{arom}), 118.6 (C_{arom}), 116.6 (CH_{arom}), 29.3 (apparent t, $J = 16$ Hz, PCHMe_2), 25.9 (apparent t, $J = 18$ Hz, PCHMe_2), 22.2 (PCHMe_2), 20.4–18.8 (overlapping resonances, PCHMe_2), 11.0 (Indole-Me), 7.2 (s with Pt satellites, $^2J_{\text{PtC}} = 60$ Hz, SiMe). $^{31}\text{P}\{^1\text{H}\}$ NMR (202.5 MHz, benzene- d_6): δ 61.2 (s with Pt satellites, $^1J_{\text{PP}} = 2692$ Hz). ^{29}Si NMR (59.6 MHz, benzene- d_6): δ 64.1 ($^1J_{\text{SiP}} = 968$ Hz, $J_{\text{SiH}} = -67$ Hz). Anal. Calcd for $\text{C}_{31}\text{H}_{46}\text{N}_2\text{P}_2\text{PtSi}$: C, 53.78; H, 7.27; N, 3.48. Found: C, 53.32; H, 7.13; N, 3.52. Although these results in % C are outside the range viewed as establishing analytical purity, they are provided to illustrate the best values obtained to date.

(Pr-P(η^2 -SiH)P^{Ind})Ni(DMAP) (4). A solution of $\{[\text{Pr-P}(\eta^2\text{-SiH})\text{P}^{\text{Ind}}]\text{Ni}\}_2(\mu\text{-N}_2)$ (0.048 g, 0.039 mmol) in benzene (ca. 5 mL) was treated with DMAP (0.009 g, 0.078 mmol) to produce a clear yellow solution. The reaction mixture was allowed to stand at room temperature for 14 h. The volatile components of the reaction mixture were subsequently removed under vacuum, and the remaining residue was washed with 2×1 mL of cold (–35 °C) pentane and dried in vacuo to afford **4** (0.055 g, 98% yield) as a bright yellow solid. ^1H NMR (500 MHz, benzene- d_6): δ 8.71 (d, $J = 7$ Hz, 2 H, H_{arom}), 8.23 (d, $J = 9$ Hz, 2 H, H_{arom}), 7.68 (d, $J = 8$ Hz, 2 H, H_{arom}), 7.28 (t, $J = 8$ Hz, 2 H, H_{arom}), 7.21 (t, $J = 8$ Hz, 2 H, H_{arom}), 5.75 (d, $J = 7$ Hz, 2 H, H_{arom}), 2.76 (m, 2 H, PCHMe_2), 2.65 (m, 2 H, PCHMe_2), 2.51 (s, 6 H, Indole-Me), 2.03 (s, 6 H, NMe_2), 1.35 (d, $^3J_{\text{HH}} = 2$ Hz, 3 H, SiMe), 1.22–1.09 (24 H, PCHMe_2), –3.50 (t, $^2J_{\text{PH}} = 40$ Hz, 1 H, Si-H-Ni). $^{13}\text{C}\{^1\text{H}\}$ NMR (125.8 MHz, benzene- d_6): δ 156.0 (CH_{arom}), 152.8 (C_{arom}), 141.1 (apparent t, $J = 6$ Hz, C_{arom}), 138.2 (apparent t, $J = 21$ Hz, C_{arom}), 135.8 (C_{arom}), 122.3 (CH_{arom}), 119.4 (CH_{arom}), 119.1 (CH_{arom}), 116.1 (C_{arom}), 115.2 (CH_{arom}), 106.2 (CH_{arom}), 38.1 (NMe_2), 29.7 (apparent t, $J = 13$ Hz, PCHMe_2), 27.9 (apparent t, $J = 6$ Hz, PCHMe_2), 21.1 (apparent t, $J = 6$ Hz, PCHMe_2), 20.6 (PCHMe_2), 20.4 (PCHMe_2), 20.1 (apparent t, $J = 5$ Hz, PCHMe_2), 11.5 (Indole-Me), 10.5 (SiMe). $^{31}\text{P}\{^1\text{H}\}$ NMR (202.5 MHz, benzene- d_6): δ 28.6. ^{29}Si NMR (99.4 MHz, benzene- d_6): δ –24.1 (d, $^1J_{\text{SiH}} = -69$ Hz). Anal. Calcd for $\text{C}_{38}\text{H}_{56}\text{N}_4\text{P}_2\text{NiSi}$: C, 63.60; H, 7.87; N, 7.81. Found: C, 63.35; H, 7.81; N, 7.57. X-ray-quality crystals of **4** were obtained from a concentrated Et_2O solution at –35 °C.

(Pr-P(η^2 -SiH)P^{Ind})Ni(PMe₃) (5a) + (Pr-PSiP^{Ind})Ni(PMe₃)H (5b). A room-temperature solution of $\{[\text{Pr-P}(\eta^2\text{-SiH})\text{P}^{\text{Ind}}]\text{Ni}\}_2(\mu\text{-N}_2)$ (0.038 g, 0.031 mmol) in benzene (ca. 5 mL) was treated with PMe_3 (0.024 g, 0.31 mmol), which was added dropwise by syringe. After standing for 2 h at room temperature, the reaction mixture was evaporated to dryness under vacuum and the remaining residue was triturated with 3×2 mL of pentane. The residue was subsequently washed with pentane (3×2 mL) to afford a ca. 2:1 mixture (by ^1H and ^{31}P NMR) of isomers **5a** and **5b** as an off-white solid (0.029 g, 70% overall yield based on Ni). Selected NMR data for **5a**: ^1H NMR (500 MHz, benzene- d_6) δ 2.38 (s, 6 H, Indole-Me), 1.48 (s, 3 H, SiMe), –5.44 (td, $^2J_{\text{PH}} = 37$ Hz, 22 Hz, 1 H, NiH); $^{13}\text{C}\{^1\text{H}\}$ NMR (125.8 MHz, benzene- d_6) δ 11.7 (Indole-Me), 9.9 (SiMe); $^{31}\text{P}\{^1\text{H}\}$ NMR (202.5 MHz, benzene- d_6) δ 42.2 (d, $^2J_{\text{PP}} = 6$ Hz, 2 P, PPr_2), –23.0 (t, $^2J_{\text{PP}} = 6$ Hz, 1 P, PMe_3); ^{29}Si NMR (99.4 MHz, benzene- d_6) δ 6.2 ($J_{\text{SiH}} = -82$ Hz). Selected NMR data for **5b**: ^1H NMR (500 MHz, benzene- d_6) δ 2.40 (s, 6 H, Indole-Me), 1.25 (s, 3 H, SiMe), –10.18 (dt, $^2J_{\text{PH}} = 49$ Hz, 38 Hz, 1 H, NiH); $^{13}\text{C}\{^1\text{H}\}$ NMR (125.8 MHz, benzene- d_6) δ 11.6 (Indole-Me), 7.5 (d, $J = 6$ Hz, SiMe); $^{31}\text{P}\{^1\text{H}\}$ NMR (202.5 MHz, benzene- d_6) δ 56.8 (d, $^2J_{\text{PP}} = 111$ Hz, 2 P, PPr_2), –19.2 (t, $^2J_{\text{PP}} = 111$ Hz, 1 P, PMe_3); ^{29}Si NMR (99.4 MHz,

benzene- d_6) δ 65.8 ($J_{\text{SiH}} = -81$ Hz). Anal. Calcd for $\text{C}_{34}\text{H}_{55}\text{N}_2\text{P}_3\text{NiSi}$: C, 60.81; H, 8.26; N, 4.17. Found: C, 60.56; H, 8.12; N, 4.01. X-ray-quality crystals of **5b** were obtained from a concentrated Et_2O solution at -35 °C.

Generation of (¹Pr-PSiP^{Ind})Ni(HCO₂) (6-Ni). A room-temperature solution of $\{[\text{Pr-P}(\eta^2\text{-SiH})\text{P}^{\text{Ind}}]\text{Ni}\}_2(\mu\text{-N}_2)$ (0.012 g, 0.010 mmol) in benzene- d_6 (ca. 1 mL) was transferred to a J. Young NMR tube and degassed via three freeze–pump–thaw cycles. CO_2 (ca. 1 atm) was introduced to the tube at ambient temperature. After 10 min at room temperature, NMR analysis of the reaction mixture indicated the quantitative formation of **6-Ni**. ^1H NMR (300 MHz, benzene- d_6): δ 8.71 (s, 1 H, HCO_2), 7.62 (apparent d, $J = 7$ Hz, 2 H, H_{arom}), 7.55 (apparent d, $J = 7$ Hz, H_{arom}), 7.17–7.11 (4 H, H_{arom}), 2.76 (m, 2 H, PCHMe_2), 2.56 (m, 2 H, PCHMe_2), 2.23 (s, 6 H, Indole-Me), 1.38–1.27 (12 H, PCHMe_2), 1.19–1.08 (12 H, PCHMe_2), 0.67 (s, 3 H, SiMe). ^{13}C NMR (75.5 MHz, benzene- d_6): δ 168.8 (HCO_2), 140.9 (apparent t, $J = 6$ Hz, C_{arom}), 137.0 (C_{arom}), 131.9 (apparent t, $J = 28$ Hz, C_{arom}), 123.2 (CH_{arom}), 121.0 (CH_{arom}), 120.4 (C_{arom}), 119.7 (CH_{arom}), 116.7 (CH_{arom}), 27.3 (apparent t, $J = 12$ Hz, PCHMe_2), 26.3 (apparent t, $J = 11$ Hz, PCHMe_2), 19.5–19.1 (overlapping resonances, PCHMe_2), 11.4 (Indole-Me), 5.2 (SiMe). $^{31}\text{P}\{^1\text{H}\}$ NMR (121.5 MHz, benzene- d_6): δ 34.6. ^{29}Si NMR (99.4 MHz, benzene- d_6): δ 42.2.

Generation of (¹Pr-PSiP^{Ind})Pd(HCO₂) (6-Pd). A room-temperature solution of **3-Pd** (0.015 g, 0.023 mmol) in benzene- d_6 (ca. 1 mL) was transferred to a J. Young NMR tube and degassed via three freeze–pump–thaw cycles. CO_2 (ca. 1 atm) was introduced to the tube at ambient temperature. After 10 min at room temperature, NMR analysis of the reaction mixture indicated the formation of **6-Pd** as the major product. Selected NMR data for **6-Pd**: ^1H NMR (300 MHz, benzene- d_6) δ 9.26 (s, 1 H, HCO_2), 2.20 (s, 6 H, Indole-Me), 0.65 (s, 3 H, SiMe); $^{31}\text{P}\{^1\text{H}\}$ NMR (121.5 MHz, benzene- d_6) δ 39.0.

General Conditions for Catalytic Hydroboration of CO_2 . For all catalytic runs using HBPIn or HBCat, the total reaction volume was kept a constant 872 μL (combined volume of borane and solvent). Unless otherwise stated, reactions were performed at room temperature for 1 h. If any precipitate was observed over the course of the reaction, excess deuterio solvent was added immediately prior to NMR data acquisition, to ensure that all reaction components were solubilized. For the more dilute reactions, the amounts of catalyst and HBPIn were decreased, and the volume difference was made up with added benzene- d_6 . Due to solubility issues, catalytic runs involving **9-BBN** were performed at a concentration of 0.96 M in **9-BBN** monomer. In a typical catalysis run (Table 2, entry 1), 0.005 g (0.0041 mmol) of $\{[\text{Pr-P}(\eta^2\text{-SiH})\text{P}^{\text{Ind}}]\text{Ni}\}_2(\mu\text{-N}_2)$ (delivered as a 100 μL aliquot of a 0.041 M stock solution of $\{[\text{Pr-P}(\eta^2\text{-SiH})\text{P}^{\text{Ind}}]\text{Ni}\}_2(\mu\text{-N}_2)$ in benzene- d_6) was added to 0.0054 g of C_6Me_6 (the internal standard) in a 1 dram vial. Benzene- d_6 (162 μL) and HBPIn (610 μL , 4.20 mmol) were added to the reaction mixture, and the combined mixture was subsequently transferred to a 250 mL Teflon-sealed reaction vessel. The solution was degassed via three freeze–pump–thaw cycles and subsequently exposed to ca. 1 atm of CO_2 for 3 min at ambient temperature, after which the reaction vessel was sealed. The reaction mixture was stirred for 1 h at room temperature, during which time a precipitate (subsequently identified as $(\text{PinBO})_2\text{CH}_2$, **7-B**) separated from solution. Benzene- d_6 (ca. 1 mL) was added to the reaction vessel to dissolve all reaction components, and the conversion to $(\text{PinBO})_2\text{CH}_2$ (**7-B**) was determined to be 84% (average of two runs) on the basis of ^1H NMR spectroscopic analysis relative to the internal standard.

Synthesis and Isolation of $(\text{PinBO})_2\text{CH}_2$ (7-B). In a typical optimized catalysis run (Table 3, entry 1), 0.005 g (0.0041 mmol) of $\{[\text{Pr-P}(\eta^2\text{-SiH})\text{P}^{\text{Ind}}]\text{Ni}\}_2(\mu\text{-N}_2)$ (delivered as a 100 μL aliquot of a 0.041 M stock solution of $\{[\text{Pr-P}(\eta^2\text{-SiH})\text{P}^{\text{Ind}}]\text{Ni}\}_2(\mu\text{-N}_2)$ in benzene- d_6) was added to 0.0054 g of C_6Me_6 (the internal standard) in a 1 dram vial. Benzene- d_6 (162 μL) and HBPIn (610 μL , 4.20 mmol) were added to the reaction mixture, and the combined mixture was subsequently transferred to a 250 mL Teflon-sealed reaction vessel. The solution was degassed via three freeze–pump–thaw cycles and subsequently exposed to ca. 1 atm of CO_2 for 3 min at ambient temperature, after which the reaction vessel was sealed. The reaction

mixture was stirred for 4 h at room temperature, during which time a precipitate separated from solution. Benzene- d_6 (ca. 1 mL) was added to the reaction vessel to dissolve all reaction components, and the conversion to **7-B** was determined to be 96% (this represents one of the two runs averaged to obtain 97% conversion to **7-B** as shown in Table 3, entry 1) on the basis of ^1H NMR spectroscopic analysis relative to the internal standard. The volatile components of the reaction mixture were removed in vacuo, and the remaining white residue consisting of **7-B** was washed with 3×1 mL of cold (-35 °C) pentane and dried under vacuum, thus affording an initial crop of **7-B**. The pentane washes were combined, from which additional **7-B** was collected by crystallization at -35 °C. Compound **7-B** was isolated as a white solid in 71% combined yield (0.45 g, 1.50 mmol). ^1H NMR (500 MHz, benzene- d_6): δ 5.51 (s, 2 H, CH_2), 1.01 (s, 24 H, CH_3). ^{11}B NMR (160.5 MHz, benzene- d_6): δ 22.8. $^{13}\text{C}\{^1\text{H}\}$ NMR (125.8 MHz, benzene- d_6): δ 85.7 (CH_2), 82.9 (CMe_2), 24.6 (CMe_2). Anal. Calcd for $\text{C}_{13}\text{H}_{26}\text{B}_2\text{O}_6$: C, 52.05; H, 8.74. Found: C, 51.87; H, 8.60.

Generation of $\text{CH}_2=\text{N}(\text{2,6-}^i\text{Pr}_2\text{C}_6\text{H}_3)$. Compound **7-B** (0.032 g, 0.11 mmol) and ferrocene (0.034 g, 0.18 mmol) were dissolved in benzene- d_6 (750 μL), and neat $\text{H}_2\text{N}(\text{2,6-}^i\text{Pr}_2\text{C}_6\text{H}_3)$ (20 μL , 0.11 mmol) was added via syringe to the solution. The reaction mixture was subsequently transferred to an NMR tube. After standing for 24 h at room temperature, 86% conversion to $\text{2,6-}^i\text{Pr}_2\text{C}_6\text{H}_3\text{NCH}_2$ was observed, as determined by ^1H NMR integration relative to the ferrocene internal standard. ^1H NMR (300 MHz, benzene- d_6) δ : 7.25 (d, 1 H, $^2J_{\text{HH}} = 18$ Hz, CH_2), 7.09–7.01 (overlapping resonances, 3 H, H_{arom}), 6.85 (d, 1 H, $^2J_{\text{HH}} = 18$ Hz, CH_2), 2.96 (sept, 2 H, $^3J_{\text{HH}} = 7$ Hz, CHMe_2), 1.11 (d, 6 H, $^3J_{\text{HH}} = 7$ Hz, CHMe_2). These NMR data are consistent with those reported previously.^{6e}

Generation of $[\text{Ph}(\text{Me})\text{N}]_2\text{CH}_2$. Compound **7-B** (0.026 g, 0.087 mmol) and ferrocene (0.017 g, 0.091 mmol) were dissolved in benzene- d_6 (750 μL), and neat HMeNPh (19 μL , 0.18 mmol) was added via syringe to the solution. The reaction mixture was subsequently transferred to an NMR tube. After standing for 24 h at room temperature, 79% conversion to $[\text{Ph}(\text{Me})\text{N}]_2\text{CH}_2$ was observed, as determined by ^1H NMR integration relative to the ferrocene internal standard. ^1H NMR (500 MHz, benzene- d_6) δ : 7.18 (m, 4 H, H_{arom}), 6.79 (apparent t, 2 H, $J = 8$ Hz, H_{arom}), 6.68 (d, 4 H, $J = 8$ Hz, H_{arom}), 4.33 (s, 2 H, CH_2), 2.48 (s, 6 H, NMe). These NMR data are consistent with those reported previously.^{6e}

Generation of $\text{PinBOCH}_2\text{PPh}_2$ and $\text{Ph}(\text{H})\text{NCH}_2\text{PPh}_2$. Compound **7-B** (0.026 g, 0.087 mmol) and ferrocene (0.022 g, 0.12 mmol) were dissolved in benzene- d_6 (750 μL), and neat HPPH_2 (15 μL , 0.086 mmol) was added via syringe to the solution. The reaction mixture was subsequently transferred to an NMR tube. After standing for 24 h at room temperature, 82% conversion to $\text{PinBOCH}_2\text{PPh}_2$ was observed, as determined by ^1H NMR integration relative to the ferrocene internal standard. Neat H_2NPh (20 μL , 0.22 mmol) was subsequently added to the reaction mixture. The resulting solution was allowed to stand at room temperature for 48 h to obtain $\text{PhNHCH}_2\text{PPh}_2$ in 78% yield relative to initial **7-B** (>95% conversion relative to $\text{PinBOCH}_2\text{PPh}_2$), as determined by ^1H NMR integration relative to the ferrocene internal standard. NMR data for $\text{PinBOCH}_2\text{PPh}_2$: ^1H NMR (500 MHz, benzene- d_6) δ 7.56–7.52 (m, 4 H, H_{arom}), 7.09–7.02 (overlapping resonances, 6 H, H_{arom}), 4.74 (d, 2 H, $^2J_{\text{PH}} = 7$ Hz, CH_2), 0.96 (s, 12 H, CH_3). ^{11}B NMR (160.5 MHz, benzene- d_6): δ 22.7; $^{13}\text{C}\{^1\text{H}\}$ NMR (125.8 MHz, benzene- d_6) δ 136.8 (d, $J = 13$ Hz, C_{arom}), 133.9 (d, $J = 19$ Hz, CH_{arom}), 128.8 (CH_{arom}), 128.7 (d, $J = 6$ Hz, CH_{arom}), 82.8 (CMe_2), 65.4 (d, $^1J_{\text{PC}} = 13$ Hz, CH_2), 24.6 (CMe_2); $^{31}\text{P}\{^1\text{H}\}$ NMR (202.5 MHz, benzene- d_6) δ -11.7. NMR data for $\text{PhNHCH}_2\text{PPh}_2$: ^1H NMR (300 MHz, benzene- d_6) δ 7.39 (m, 4 H, H_{arom}), 7.15–7.01 (overlapping resonances, 8 H, H_{arom}), 6.74 (apparent t, 1 H, $J = 8$ Hz, H_{arom}), 6.41 (d, 2 H, $J = 8$ Hz, H_{arom}), 3.61 (m, 2 H, CH_2), 3.48 (broad s, 1 H, NH), 1.01 (s, 12 H, CMe_2); $^{31}\text{P}\{^1\text{H}\}$ NMR (121.5 MHz, benzene- d_6) δ -19.3. The NMR data for $\text{Ph}(\text{H})\text{NCH}_2\text{PPh}_2$ are consistent with those reported previously.²⁴

Crystallographic Solution and Refinement Details. Crystallographic data were obtained between 173(2) and 193(2) K on either a Bruker D8/APEX II CCD or a Bruker PLATFORM/APEX II CCD

diffractometer equipped with a CCD area detector using graphite-monochromated Mo $K\alpha$ ($\lambda = 0.71073$ Å) radiation (except for **2-Ni** and **5b**, where Cu $K\alpha$, $\lambda = 1.54184$ Å, radiation was used) employing samples that were mounted in inert oil and transferred to a cold gas stream on the diffractometer. Programs for diffractometer operation, data collection, and data reduction (including SAINT) were supplied by Bruker. Data reduction, correction for Lorentz–polarization, and absorption correction were each performed. Structure solution was achieved by either intrinsic phasing methods or Patterson search/structure expansion. All structures were refined by use of full-matrix least-squares procedures (on F_o^2) with R1 based on $F_o^2 \geq 2\sigma(F_o^2)$ and wR2 based on $F_o^2 \geq -3\sigma(F_o^2)$. Unless otherwise indicated, all non-hydrogen atoms were refined with anisotropic displacement parameters. In the case of **1**, disorder involving the isopropyl group comprised of C(440)–C(46) and the Si–Me group (C(1)) was identified. Each of the carbon atoms in question was refined anisotropically over two positions (A and B) with occupancy factors of 0.5. In the case of both **2-Pt** and **4**, the crystal used for data collection was found to display nonmerohedral twinning. In each case, both components of the twin were indexed with the program CELL_NOW (Bruker AXS Inc., Madison, WI, 2004). For **2-Pt**, the second twin component can be related to the first component by 180° rotation about the [0,1,0] axis in both real space and reciprocal space. For **4**, the second twin component can be related to the first component by 180° rotation about the [0.205,0,1] axis in real space and about the [0,0,1] axis in reciprocal space. For each structure, integrated intensities for the reflections from the two twin components were written into a SHELXL-2014 HKLF 5 reflection file with the data integration program SAINT (version 8.34A), using all reflection data (exactly overlapped, partially overlapped, and nonoverlapped). The refined value of the twin fraction (SHELXL-2014 BASF parameter) for **2-Pt** was 0.3(5), while for **4** the value was 0.1137(4). Disorder involving the isopropyl groups was also identified for **2-Pt**, such that each of C(31)–C(33), C(41)–C(43), and C(44)–C(46) were refined isotropically over two positions (A and B) with occupancy factors of 0.5. C(44A) and C(44B) were refined with common isotropic displacement parameters. C(35) was refined anisotropically over two positions (A and B) with occupancy factors of 0.5. The following pairs of distances were constrained to be equal (within 0.01 Å) during refinement: $d(\text{P}(1)\text{--C}(31\text{A})) = d(\text{P}(1)\text{--C}(31\text{B}))$; $d(\text{P}(2)\text{--C}(44\text{A})) = d(\text{P}(2)\text{--C}(44\text{B}))$. One equivalent of Et₂O was located in the asymmetric unit for **2-Pt**. Disorder involving this Et₂O molecule was addressed in a satisfactory manner by refinement of the non-hydrogen atoms over two positions (O(1SA), C(1SA)–C(4SA) with an occupancy factor of 0.65, and O(1SB), C(1SB)–C(4SB) with an occupancy factor of 0.35) with a common isotropic displacement parameter. The following constraints were applied to distances within the disordered Et₂O molecule: $d(\text{O}(1\text{SA})\text{--C}(1\text{SA})) = d(\text{O}(1\text{SA})\text{--C}(3\text{SA})) = d(\text{O}(1\text{SB})\text{--C}(1\text{SB})) = d(\text{O}(1\text{SB})\text{--C}(3\text{SB})) = 1.45(1)$ Å; $d(\text{C}(1\text{SA})\text{--C}(2\text{SA})) = d(\text{C}(3\text{SA})\text{--C}(4\text{SA})) = d(\text{C}(1\text{SB})\text{--C}(2\text{SB})) = d(\text{C}(3\text{SB})\text{--C}(4\text{SB})) = 1.52(1)$ Å; $d(\text{O}(1\text{SA})\cdots\text{C}(2\text{SA})) = d(\text{O}(1\text{SA})\cdots\text{C}(4\text{SA})) = d(\text{O}(1\text{SB})\cdots\text{C}(2\text{SB})) = d(\text{O}(1\text{SB})\cdots\text{C}(4\text{SB})) = 2.42(1)$ Å; $d(\text{C}(1\text{SA})\cdots\text{C}(3\text{SA})) = d(\text{C}(1\text{SB})\cdots\text{C}(3\text{SB})) = 2.35(1)$ Å. In the case of **4**, two crystallographically independent molecules of [Pr-P(η^2 -SiH)P^{Ind}]₂Ni(DMAP) (A and B) and 1.5 equiv of Et₂O were located in the asymmetric unit; for convenience, only molecule A is discussed in the text. Disorder involving the Et₂O solvate was noted during the refinement process for **4**; this disorder was treated in a satisfactory manner by employing a model featuring one fully occupied Et₂O molecule that was refined anisotropically without difficulty and a half-occupied and inversion-disordered Et₂O solvate (O(2S) and C(5S)–C(8S), refined isotropically) within the asymmetric unit. The disordered solvate was restrained to have the same approximate geometry as the well-behaved solvate by use of the SHELXL SAME instruction. The Si–H in **1** was located in the difference map, and disorder involving the hydride was addressed in a satisfactory manner by refinement of the hydrogen atom over two positions (H(1A), with an occupancy factor of 0.75, and H(1B), with an occupancy factor of 0.25) with a common isotropic displacement parameter. The Si–H(1A) and Si–H(1B) distances were constrained to be equal (within

0.03 Å) during refinement. The Ni–H groups in **4** and **5b** were each located in the difference map and refined isotropically. Otherwise, all hydrogen atoms were added at calculated positions and refined by use of a riding model employing isotropic displacement parameters based on the isotropic displacement parameter of the attached atom. Additional crystallographic details are available in the deposited CIFs (CCDC 1558787–1558792).

■ ASSOCIATED CONTENT

Supporting Information

The Supporting Information is available free of charge on the ACS Publications website at DOI: 10.1021/acs.organomet.7b00497.

NMR spectra, including variable-temperature data (PDF)

Accession Codes

CCDC 1558787–1558792 contain the supplementary crystallographic data for this paper. These data can be obtained free of charge via www.ccdc.cam.ac.uk/data_request/cif, or by emailing data_request@ccdc.cam.ac.uk, or by contacting The Cambridge Crystallographic Data Centre, 12 Union Road, Cambridge CB2 1EZ, UK; fax: +44 1223 336033.

■ AUTHOR INFORMATION

Corresponding Author

*E-mail for L.T.: laura.turculet@dal.ca.

ORCID

Robert McDonald: 0000-0002-4065-6181

Michael Ferguson: 0000-0002-5221-4401

Laura Turculet: 0000-0002-2499-5343

Notes

The authors declare no competing financial interest.

■ ACKNOWLEDGMENTS

We are grateful to the Natural Sciences and Engineering Research Council (NSERC) of Canada, the Killam Trusts, and Dalhousie University for their support of this work. We also thank Prof. Georgii Nikonov (Brock University) for helpful discussions.

■ REFERENCES

- (1) *Carbon Dioxide as Chemical Feedstock*; Aresta, M., Ed.; Wiley-VCH: Weinheim, Germany, 2010.
- (2) For selected reviews of CO₂ reduction chemistry, see: (a) Braunstein, P.; Matt, D.; Nobel, D. *Chem. Rev.* **1988**, *88*, 747–764. (b) Leitner, W. *Angew. Chem., Int. Ed. Engl.* **1995**, *34*, 2207–2221. (c) Jessop, P. G.; Ikariya, T.; Noyori, R. *Chem. Rev.* **1995**, *95*, 259–272. (d) Sakakura, T.; Choi, J.-C.; Yasuda, H. *Chem. Rev.* **2007**, *107*, 2365–2387. (e) Cokoja, M.; Bruckmeier, C.; Rieger, B.; Herrmann, W. A.; Kuhn, F. E. *Angew. Chem., Int. Ed.* **2011**, *50*, 8510–8537.
- (3) (a) Zhang, L.; Hou, Z. *Chem. Sci.* **2013**, *4*, 3395–3403. (b) Chong, C. C.; Kinjo, R. *ACS Catal.* **2015**, *5*, 3238–3259. (c) Bontemps, S. *Coord. Chem. Rev.* **2016**, *308*, 117–130.
- (4) For examples of CO₂ hydroboration to the formic acid level, see: (a) Shintani, R.; Nozaki, K. *Organometallics* **2013**, *32*, 2459–2462. (b) Suh, H. W.; Guard, L. M.; Hazari, N. *Chem. Sci.* **2014**, *5*, 3859–3872.
- (5) For examples of CO₂ hydroboration to the methanol level, see: (a) Chakraborty, S.; Zhang, J.; Krause, J. A.; Guan, H. *J. Am. Chem. Soc.* **2010**, *132*, 8872–8873. (b) Sgro, M. J.; Stephan, D. W. *Angew. Chem., Int. Ed.* **2012**, *51*, 11343–11345. (c) Courtemanche, M. A.; Legare, M. A.; Maron, L.; Fontaine, F. G. *J. Am. Chem. Soc.* **2013**, *135*, 9326–9329. (d) Anker, M. D.; Arrowsmith, M.; Bellham, P.; Hill, M. S.; Kociok-Köhn, G.; Liptrot, D. J.; Mahon, M. F.; Weetman, C. *Chem. Sci.* **2014**, *5*, 2826. (e) Wang, T.; Stephan, D. W. *Chem. Commun.*

2014, 50, 7007–7010. (f) Pal, R.; Groy, T. L.; Trovitch, R. J. *Inorg. Chem.* **2015**, 54, 7506–7515.

(6) For examples of CO₂ hydroboration to the formaldehyde level, see: (a) Bontemps, S.; Vendier, L.; Sabo-Etienne, S. *Angew. Chem., Int. Ed.* **2012**, 51, 1671–1674. (b) Bontemps, S.; Sabo-Etienne, S. *Angew. Chem., Int. Ed.* **2013**, 52, 10253–10255. (c) Bontemps, S.; Vendier, L.; Sabo-Etienne, S. *J. Am. Chem. Soc.* **2014**, 136, 4419–4425. (d) Suh, H.-W.; Guard, L. M.; Hazari, N. *Polyhedron* **2014**, 84, 37–43. (e) Jin, G.; Werncke, C. G.; Escudie, Y.; Sabo-Etienne, S.; Bontemps, S. *J. Am. Chem. Soc.* **2015**, 137, 9563–9566.

(7) While the reduction of CO₂ to methane with borane reducing agents has not yet been reported, such transformations have been realized via hydrosilylation. For selected examples, see: (a) Matsuo, T.; Kawaguchi, H. *J. Am. Chem. Soc.* **2006**, 128, 12362–12363. (b) Berkefeld, A.; Piers, W. E.; Parvez, M. *J. Am. Chem. Soc.* **2010**, 132, 10660–10661. (c) Mitton, S. J.; Turculet, L. *Chem. - Eur. J.* **2012**, 18, 15258–15262. (d) Berkefeld, A.; Piers, W. E.; Parvez, M.; Castro, L.; Maron, L.; Eisenstein, O. *Chem. Sci.* **2013**, 4, 2152–2162. (e) Lu, Z.; Hausmann, H.; Becker, S.; Wegner, H. A. *J. Am. Chem. Soc.* **2015**, 137, 5332–5335.

(8) (a) Wang, Z. C.; Diel, N.; Kretschmer, R.; Ma, J. B.; Weiske, T.; Schlangen, M.; Schwarz, H. *Angew. Chem., Int. Ed.* **2012**, 51, 3703–3707. (b) Heim, L. E.; Konnerth, H.; Precht, M. H. G. *Green Chem.* **2017**, 19, 2347–2355.

(9) Huang, F.; Zhang, C.; Jiang, J.; Wang, Z. X.; Guan, H. *Inorg. Chem.* **2011**, 50, 3816–3825.

(10) Hazari and co-workers^{6d} reported CO₂ hydroboration catalyzed by [κ^3 -(2-Ph₂PC₆H₄)₂SiMe]Ni(η^3 -C₈H₁₃) to a variety of products, including (PinBO)₂CH₂. However, over time, 85% conversion to (PinB)₂O, 13% PinBOMe, an unquantified amount of formaldehyde, and other unidentified products were observed.

(11) (a) MacLean, D. F.; McDonald, R.; Ferguson, M. J.; Caddell, A. J.; Turculet, L. *Chem. Commun.* **2008**, 5146–5148. (b) Morgan, E.; MacLean, D. F.; McDonald, R.; Turculet, L. *J. Am. Chem. Soc.* **2009**, 131, 14234–14236.

(12) Wassenaar, J.; Reek, J. N. *Dalton Trans.* **2007**, 34, 3750–3753.

(13) (a) Mitton, S. J.; McDonald, R.; Turculet, L. *Angew. Chem., Int. Ed.* **2009**, 48, 8568–8571. (b) Mitton, S. J.; McDonald, R.; Turculet, L. *Organometallics* **2009**, 28, 5122–5136.

(14) Suh, H.-W.; Schmeier, T. J.; Hazari, N.; Kemp, R. A.; Takase, M. K. *Organometallics* **2012**, 31, 8225–8236.

(15) Crabtree, R. H. *The Organometallic Chemistry of the Transition Metals*, 6th ed.; Wiley: Hoboken, NJ, 2014.

(16) Corey, J. Y. *Chem. Rev.* **2011**, 111, 863–1071.

(17) Kozminski, W.; Nanz, D. *J. Magn. Reson.* **1997**, 124, 383–392.

(18) For related examples of η^2 -SiH coordination involving PSiP ligation, see: (a) Takaya, J.; Iwasawa, N. *Organometallics* **2009**, 28, 6636–6638. (b) Takaya, J.; Iwasawa, N. *Dalton Trans.* **2011**, 40, 8814–8821. (c) Charboneau, D. J.; Balcells, D.; Hazari, N.; Lant, H. M. C.; Mayer, J. M.; Melvin, P. R.; Mercado, B. Q.; Morris, W. D.; Repisky, M.; Suh, H.-W. *Organometallics* **2016**, 35, 3154–3162. See also ref 14.

(19) The interconversion between terminal M^{II}-H and (η^2 -SiH)-M⁰ complexes involves hydride transfer between the metal center and Si; for related alkyl and aryl group transfer involving Ni and Pd complexes supported by κ^3 -(2-R₂PC₆H₄)₂SiMe ligation, see refs 4b, 13a, and 18a.

(20) (a) Ignatov, S. K.; Rees, N. H.; Tyrrell, B. R.; Dubberley, S. R.; Razuvaev, A. G.; Mountford, P.; Nikonov, G. I. *Chem. - Eur. J.* **2004**, 10, 4991–4999. (b) Nikonov, G. I. *Adv. Organomet. Chem.* **2005**, 53, 217–309.

(21) Suh, H. W.; Balcells, D.; Edwards, A. J.; Guard, L. M.; Hazari, N.; Mader, E. A.; Mercado, B. Q.; Repisky, M. *Inorg. Chem.* **2015**, 54, 11411–11422.

(22) Wu, S.; Li, X.; Xiong, Z.; Xu, W.; Lu, Y.; Sun, H. *Organometallics* **2013**, 32, 3227–3237.

(23) For other examples of CO₂ functionalization see: (a) Federsel, C.; Boddien, A.; Jackstell, R.; Jennerjahn, R.; Dyson, P. J.; Scopelliti, R.; Laurenczy, G.; Beller, M. *Angew. Chem., Int. Ed.* **2010**, 49, 9777–

9780. (b) Tsuji, Y.; Fujihara, T. *Chem. Commun.* **2012**, 48, 9956–9964. (c) Blondiaux, E.; Pouessel, J.; Cantat, T. *Angew. Chem., Int. Ed.* **2014**, 53, 12186–12190. (d) Li, Y.; Cui, X.; Dong, K.; Junge, K.; Beller, M. *ACS Catal.* **2017**, 7, 1077–1086. See also refs 2a, e, and 4a.

(24) Payet, E.; Auffrant, A.; Le Goff, X. F.; Floch, P. L. *J. Organomet. Chem.* **2010**, 695, 1499–1506.